Department of Precision and Microsystems Engineering

Modelling the axis drift of short wire flexures and increasing their support stiffness using polymers, and the application to the Delta Robot

Boris Daan

Report no : 2020.053
Coach : Ir. J. Rommers
Professor : Prof. dr. ir. J.L. Herder
Specialisation : Mechatronic System Design
Type of report : Master Thesis
Date : 24 November 2020

TU Delft Delft University of Technology

CODIAN ROBOTICS

Challenge the future

Preface

This thesis concludes my master High Tech Engineering (HTE) at the faculty of Mechanical, Maritime and Material Engineering (3mE) at the Delft University of Technology. I am proud to graduate at one of the most technical disciplines here at Delft University of Technology.

I would like to thank my supervisors from the TU Delft, Jelle Rommers and Just Herder, for their support, useful feedback, and weekly meetings to keep me on track throughout the year. I would also like to thank my fellow students joining these weekly meetings for their ideas and feedback. Then, for the countless hours of studying together and keeping each other motivated, thanks to Pim Vugts.

I would like to thank Codian Robotics for the means to make this thesis a reality. Thanks to Wesley Donselaar, Charl Claassen, and Frank Franssen for their help and support.

Finally, I would like to thank my parents, girlfriend, family, and friends for their continuous support.

Boris Daan
Delft, November 2020

Contents

Chapter 1

Introduction

This thesis focuses on the development of flexure joints for a delta robot, a pick and place robot mainly used in the packaging industry. This research is the result of the collaboration of the Technical University Delft and Codian Robotics. Codian Robotics designs and builds delta robots, which up to now use ball joints for the connections between the different parts of the robot. Replacing these ball joints with flexures could result in a lighter, cheaper and faster robot made from fewer parts. Next to this, flexures can limit the number of creases and pockets that could accumulate dirt or bacteria. This benefits delta robots, as they are often used in dirty environments, or environments where hygiene is important such as the food industry. Therefore, the goal for this thesis is to develop a flexure that can be used in the delta robot to replace the ball joint, while increasing hygiene and performance.

1.1 Research objectives

Due to the high accelerations on a delta robot, flexures with high support stiffness over a large range of motion are required to remain precise in their outputs. Due to the small amount of strain allowed in steel, complex flexure geometries are required to reach high support stiffness. However, these complex geometries have creases or pockets which are undesired. As polymers allow large amounts of strain, their use for flexures is investigated to create simple wire flexures with high support stiffness over large ranges of motion. However, when bending the wire flexure, it does not rotate around a fixed point such as the ball joint, but has axis drift. As the delta robot is feed-forward controlled, this limits the accuracy of the system. A new method to model the axis drift of wires is investigated.

1.2 Thesis outline

Chapter 2 focuses on the literature research on the subject of delta robots and flexure designs. In chapter 3, the paper that forms the main part of this research is presented on the modelling of axis drift of wire flexures and increasing support stiffness by using polymers. The project is then discussed in chapter 4 and concluded in chapter 5. The appendices then expand on the following: A: improving the accuracy of the pseudo-rigid-body model (PRBM) with characteristic pivot, B: the design process of the flexure hinges, C: the application of the arc method to the delta robot, D: a separate design for a compliant rotation arm of the delta robot, and E: the testing setups used.

Chapter 2

Literature Study

2.1 Introduction

First, in this introduction the different aspects of the literature research are introduced, and a research objective is given. In section 2.2, a problem analysis is done on replacing the joints in a delta robot. Section 2.3 then gives an overview the research that already has been done in this field. Finally, the literature study is concluded in section 2.4.

2.1.1 Pick and Place Robots

During production and packaging, for instance in the food industry, products need to be picked up and placed to continue the process. They go from one conveyor belt to the next, or into their packaging. To do this efficiently, different types of robots have been designed. If the focus is on a single type of product, maybe a specialised machine just for that product could do the job the fastest. An example of this can be seen in figure 2.1a. A problem here is limited flexibility in placement actions or product selection. A more standard robot such as the delta robot could still do the job effectively, but with a lot more versatility.

(a) Industrial bottle filling and handling machine [1]

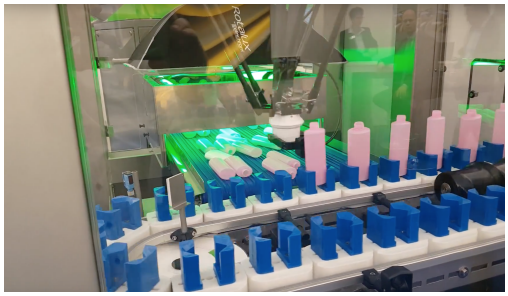

(b) A Delta robot used in the handling of bottles [2]

Figure 2.1: Bottle handling machines

2.1.2 Parallel and Serial Robots

The most used types of pick and place robots in the industry can be divided into two categories, parallel and serial robots. Serial mechanisms use multiple links in series to get the wanted degrees of freedom (DOF), like the robotic arm, Scara, and Cartesian robots. Parallel robots use multiple links in parallel, together constraining the DOF. Parallel robots pose an advantage over serial robots in stiffness and precision, as errors are averaged instead of stacked like serial robots. Because of these characteristics, parallel robots are well suited to work with compliant joints.

2.1.3 Delta Robots

In the pick and place industry, the most used parallel robot is the Delta robot, initially designed specifically for this task, namely for putting chocolates into their boxes [3]. In contrast to most other pick and place robots, the structure of the delta robot allows for statically mounted motors. All of the input motors and gear housings are connected to the base, resulting in a very low weight moving mass. This makes the Delta robot suitable for high accelerations during the pick and place actions.

(a) A D2 Delta robot, with the additional linkages to form parallelograms

(b) A D4 Delta robot with 4 DOF, a rotation arm added.

Figure 2.2: Different types of Delta robots made by Codian Robotics

Working Principle

Delta robots use a system of parallelograms connected to three input arms to position the end-effector in 3D space. Because of the parallelograms, the end-effector always stays parallel to the base, thus only having 3DOF. Each of the joints between the input arms, parallelogram linkages, and end effector needs to have 2DOF. Because of their stiffness and simplicity, ball joints are used. The third DOF in these joints is not used for the end effector, but allows rotation of the links of the parallelogram. Most Delta robots use springs to pretension the ball joints to increase precision. This spring is placed between the two linkages of the parallelogram and partially constraints the third DOF.

Terminology

As explained above, the standard Delta robot has 3DOF. In the original patent, an additional rotation arm in the middle of the robot was also present [4]. This adds a 4th DOF, allowing the continuous rotation of the end effector. This type of Delta robot will be referred to as *D4*. This robot can be seen in figure 2.2b. The delta robot can also be flattened to work with only 2DOF, resulting in a D2 robot in figure 2.2a. Here additional linkages are needed to form parallelogram action that keeps the end effector parallel. An additional rotation arm can also be attached on a D2 robot.

From now the input arms are referred to as *primary arms*, and the parallelogram linkages as *secondary arms*. The end effector at the bottom of the secondary arms is referred to as the *tool centre point*, or *TCP*.

2.1.4 Compliant mechanisms

Normally, compliance is seen as a bad thing for robots. A reduce in stiffness leads to lower eigenfrequencies and thus a lower control frequency. However, compliance can also be used to our advantage. When allowing the material to flex in certain ways to control the DOF of the robot, the stiffness in other directions can be maintained. In the precision industry, compliant hinges are mostly used because of their predictable behaviour due to zero backlash. Compliant hinges have some more advantages still, which are most of the time overlooked in the precision industry. Things like hygiene due to no creases and pockets, or long lifetime due to the zero friction, can be very beneficial in the pick and place industry.

2.1.5 Research Objective

The objective of this literature research is to make a comprehensive overview of the available research in this field. The different fields that are looked at are large range flexures, delta robots, and delta robots with flexures. Next to this, we will look into material choices for these flexures. Normally steel is used, but the possibilities of using polymers for flexures is also investigated.

2.2 Problem Analysis

In this section, an in depth problem analysis of the joints in a delta robot. Starting at what functions the finished product should fulfil, after which the lifetime is looked at. As the environment of the robot has a big impact on which materials can be used and how the robot is operated, different use cases are looked into.

2.2.1 Function

Based on the standard use case for the robot according to Codian, the robot must pick up an item of about 2 kg and move that item over a predefined path. The robot must then move back to the start position, ready to pick up another item. For a standard pick and place action, this happens about 120 times per minute, or 2 times per second. The precision with which this action has to be executed is different for item. 0.1 mm is the standard for the Delta robots from Codian now, but in most cases a precision of 1 mm to 5 mm suffices. The current D4 robots come in different sizes, each with their own workspace. The most popular robot has a workspace of a cylinder with a diameter of about 1 m and a height of about 0.4 m. This will be used as a baseline for the design. All these fast pick and place actions need to happen for a lifetime of a few years, with millions of repetitions.

2.2.2 Lifetime

To determine a more exact lifetime, the gearbox is looked at. It is the most expensive part of the robot, making up about half of the cost of the system. When the gearbox wears out, the precision decreases due to backlash in the teeth of the gears. When this decreased precision does not satisfy the customer anymore, usually the whole robot is replaced. The lifetime for the gearbox does change with each application, as it is dependent on the loads and use of the robot. On average, the robot has a pick and place frequency of around 2 Hz, and operates 8 hours a day for 300 days a year. For a lifetime of 5 years this means around 10^7 of pick and place actions.

2.2.3 Environment

Some of the robots work with continuous water spraying down on them, or in very dirty or otherwise contamination conditions. In addition to this, if food products are being handled, the materials used must be FDA approved. There is also a risk of bacteria or other contaminants getting into creases and or closed off parts of the machine, if they are not sealed off correctly.

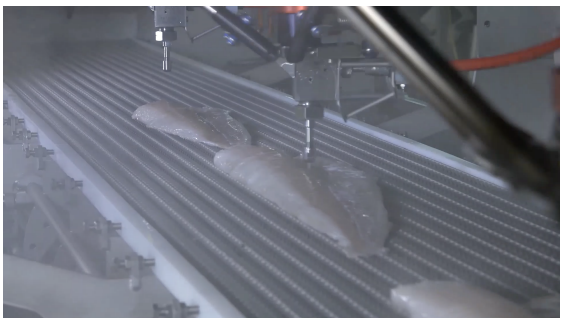

Figure 2.3: A waterjet attached to a Delta Robot, cutting out fish fillets

2.2.4 Joint types

Looking at the different types of delta robots from Codian, see figure 2.2, a few joint types can be seen. In the D4 Delta robot, a rotation joint is used for the attachment of the primary arm to the motor, gearbox, and base. During this research, this joint is not looked at. It would require a complete redesign of the motor and gearbox, which is not in the scope of this project. After that, only ball joints are used between the primary arm, secondary arm, and TCP. These can be seen in figure 2.4a. For the rotation arm, a CV or U joint is used at either end, see figure 2.4b. The linear bearing can also be seen here, which allows the rotation arm to change length while still transferring the torque to the TCP. In the D2 robot, as everything moves in one plane, the ball joints can be replaced with revolute joints, these can be seen in figure 2.4c. The rotation arm still acts in the same way, so the same joints apply here.

(a) The spring loaded ball joints of the delta robot.

(b) Rotation arm of a D4 robot, with a CV joint and linear bearing.

(c) The revolute joint used in a D2 robot.

Figure 2.4: Joint Types Delta Robots

In most cases, a 2D problem is less complex than a 3D problem. At the beginning of the project this seemed the case for the delta robots, so the plan was to first design flexures for a D2 robot, and based on the results design a flexible D4 robot. For a D2 robot, each of the joints only requires 1DOF, the main rotation. All other directions should have sufficient support stiffness, as the loading of the robot is not in 2D. This complicates the problem, as high support stiffness in all directions but one is difficult to reach with flexures.

In a D4 robot, the hinge would replace a ball joint, where all of the rotations are allowed and thus less DOF need to be constraint. This actually simplifies the problem, so this is where the research for a flexible delta robot starts.

2.2.5 Critical Stiffness Ball Joints

The TCP in a D4 robot is positioned by the rotation of the primary arms, and the length of the secondary arms. Motions that cause a change in these two values have an effect on the precision of the robot. As in this research, there is no focus on the primary arms, only the length of the secondary arms in looked at. In the two ball joints at either end, all rotations are allowed. Translations in the joint are not allowed, and lower the precision of the system. However, translations perpendicular to the rod cause only a minimal change in length of the secondary arms, so the main focus is on the stiffness of the flexures inline with the rods.

2.2.6 Advantages Compliant Joint

In the case of the robots from Codian, the cup covers only half of the ball, and is force closed. This reduces play but increases friction and stiction.

Stainless steel is used for the balls, which does not wear much over the lifetime of the machine. For all machines that are not used in the food industry, Nylatron cups are used, as they offer the best wear resistance but are not FDA approved [5]. They are inserted into the housing, and can be replaced if necessary, although they also are very wear-resistant. However, when the machine is used in the food industry, FDA approved cups have to be used [6]. These cups wear a lot quicker, and have to be replaced multiple times during the lifespan of the robot. To conclude, ball-joints have the following disadvantages, stated below:

- *Friction* - The ball and socket of the joint move over each other, which will always cause some sort of friction. Choosing proper materials or lubrication will reduce this friction, but can never completely remove it. Friction increases input forces and creates heat in the system.

- *Stiction* - Again, as two parts move over each other, there is also stiction. Stiction reduces precision and to some amount also the control frequency.

- *Wear* - As the joints have friction, there is also always some wear. Using easily replaceable inserts makes the wear serviceable, but limits uptime of the robot. With constant lubrication, this wear can also be counteracted, but in the use case of these Delta robots this almost never possible.

- *Particle generation* - The material removed by the wear of the joints has to go somewhere. Small particles of the material can end up in the product the delta robot is moving.

- *Creases* - Not only can particles come out of this system, because of the crease between the two parts foreign material can also get stuck in between the ball and socket. This could either damage the joint or create a spot where (biological) residue could compromise the hygiene of the product.

Compliant joints can do better in all of these points, and on top of that reduce part count and cost and weight. This does come with some other disadvantages, which the ball joint does not have

- *Stiffness* - As the compliant joint has to flex in some directions but be stiff in others, a compromise has to be made. Geometries can be altered to increase this support stiffness, but it is probable that this support stiffness will decrease with respect to the ball joints.

- *Rotation Centre* - A ball joint has a very defined rotation centre, which makes the kinematic model for the robot very well defined. In combination with the high support stiffness, the Delta robot can be very easily feed-forward controlled. Most compliant links see a shift in rotation centre over the travel of the joint. Especially for large deflections, this centre can shift drastically.

2.2.7 Requirements and Wishes

Requirement type	Specification
Size	Maximum size 13mm, must fit in tubes, fit on TCP
Working range	1100x400mm
Motion range	Minimum motion range of 70° to each side.
Controlling frequency	minimum frequency of 120 picks per minute
Payload	minimum payload of 2 kg
Accelerations	Minimum acceleration/deceleration of 3 g with payload of 2 kg
Strength	Must withstand forces of 60 newton in all directions
Stiffness/eigenfrequency	Minimum parasitic eigenfrequency for control of Hz
Lifetime	Minimum placement amount of 10^7 cycles
Temperature	Working temperaturees between 0 and 50°C
repeatibility / precision	Minimum precision of 0,1 mm
shock loads	Must handle shocks (bumping into other objects)
Environment	Must work in Water/dirt conditions
Hygiene	Must be made from food-save materials/no places for dirt to accumulate/withstand detergents
Crash resistant	must be able to fail safely, only small part breaking

Wishes	specification
Mass	Low
Cost	Low
Production time	Low
Prototypebility	High

2.2.8 Objective

Replacing the ball joints with flexures could improve the delta robot performance, while reducing complexity and cost.

The goal of this thesis is to find a hinge type that can withstand millions of repetitions without failure, whilst bending more than 70° to every side. On top of this, the hinge should be easy to clean and be strong and stiff enough for pick and place actions. When used in a delta robot, this results in a robot with a workspace of a cylinder with a diameter of about 1 m and a height of about 0.4 m.

2.3 State of the art

2.3.1 Delta Robots

So as explained in the introduction, a Delta robot is a type of parallel robot. Parallel robots use multiple links from base to the end-effector, together constraining the DOF. The structure of the delta robot allows for statically mounted motors, lowering the moving mass. The first Delta robot was designed by Raymond Clavel, which was patented in 1989 [4].

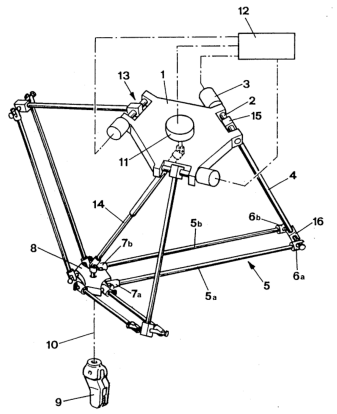

(a) The drawing of the Delta structure from the original patent [4]

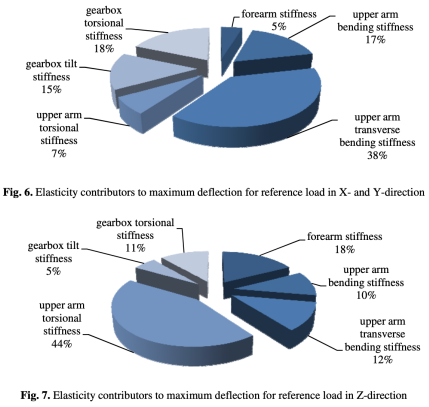

(b) How each part of the robot contributes to the compliance [7]

Figure 2.5

Over the years, multiple studies have focused on the Delta robot. Optimising the kinematic structure for a given workspace[8], or on how to control a Delta robot at high speed [9]. Both of these studies might be useful in a later stage of the research, when the Delta robot has to be altered and controlled for a well-working flexure hinge. A research that is very useful now is the one of Wahle (2011) [7]. Here the stiffness of the end effector is looked at over the entire range of the Delta robot. The different links in the system are all looked at, and each of their contribution to the compliance of the system is listed. This results in the graphs in figure 2.5b. Here can be seen that the secondary or forearms contribute very little to both the X, Y, and Z compliance of the robot. This means that a lowered stiffness in the ball joints due to the flexures has a relatively small effect on the TCP stiffness.

2.3.2 Flexures

One of the most basic flexure hinges is the notch flexure. It already comes in a lot of different shapes and sizes, of which a selection is made in figure 2.6. Next to the notch flexure, the leaf flexure is also one of the basic building blocks in flexure design. There is also some overlap between the two, as a thin stretched out notch bears a lot of resemblance to a leaf flexure. Normally these flexures are only suited for small rotations, and different geometries have to be used to get to larger rotations. This is especially true if there is a need for some support stiffness of the flexure.

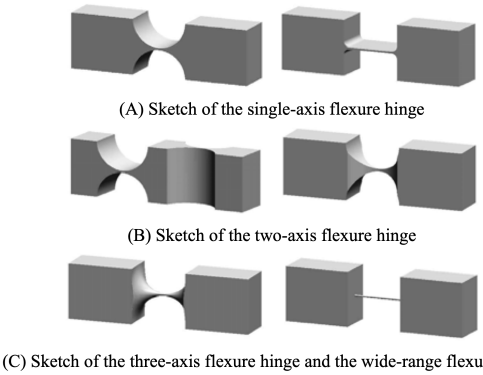

Figure 2.6: Different types of notch flexures [10]

Almost all of these flexures with more complex geometries are revolute joints, as a common problem is that flexures are used for a revolute joint where the support stiffness is critical, like in Wiersma (2014) [11]. Here hinges like the one in figure 2.7a are assessed, and their parasitic eigenfrequency plotted against the rotation angle. A large decline in support stiffness depicted in figure 2.7b, at only 20° rotation, there is already a 60% decrease in parasitic eigenfrequency. When the amount of flex necessary goes from 20° to more than 70° for a D2 delta robot, this problem becomes even more drastic. This 70° is based on a total joint rotation of about 140° used for the delta robot to move the TCP in its domain. If the TFCH as in figure 2.7a would be used in a D2 robot, they would be replacing a revolute joint and this critical support stiffness is a rotation around the x-axis.

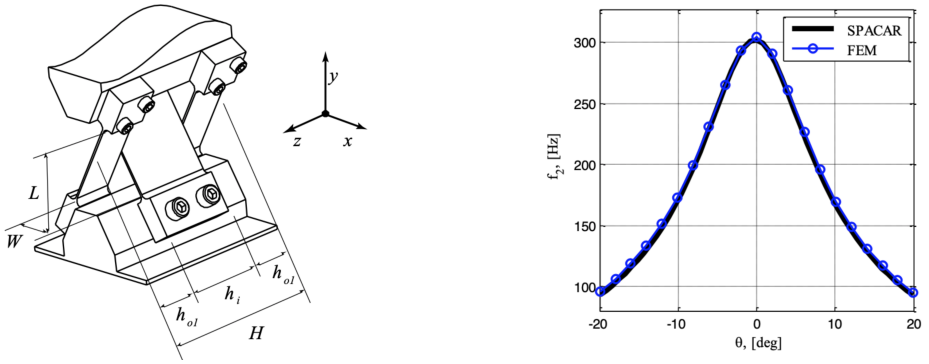

(a) Three-Flexure Cross Hinge (TFCH)

(b) Parasitic eigenfrequency as a function of the deflection angle

Figure 2.7: One of the flexures tested and optimised for parasitic eigenfrequency [11]

More complex geometries can be made still, like adding stiffeners on the flexures themselves giving a torsional reinforced leaf spring or TRLS, see figure 2.8a. Even these can be combined again to get higher support stiffness still, as depicted in figure 2.8b. Here three TRLS are stacked in series, and two guiding TFCH are placed on the outside. The problem with all these complex flexures is that they contain a lot of pockets and small spaces which are difficult to clean. In this research, cleanability and durability is a hard requirement.

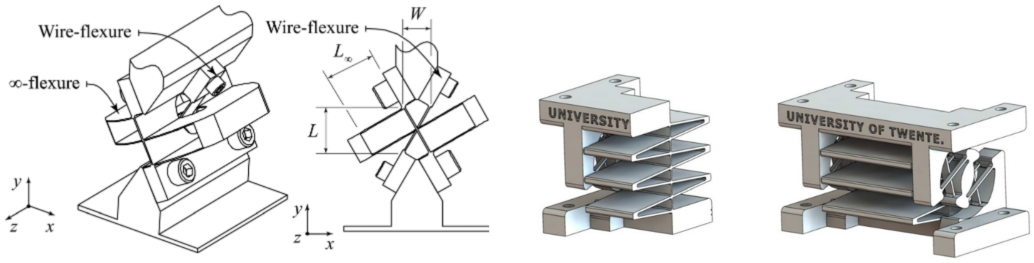

(a) The infinity flexure or TRLS, that due to stiffeners has a higher support stiffness at large deflections [11]

(b) The hinge combination of three TRLS and two double TFCH [12]

Figure 2.8: Infinity hinge designs

Even for these very complex joints, the rotations needed in the Delta robots have not been explored much in the field of compliant hinges. The research by Trease (2005) [13] does give some suitable shapes for joints that could possibly bend that far, but with the material used in the paper (ABS plastic) the joint only goes up to 27°. In most other papers, due to the precision requirements, the joints are made out of metal. Using polymers could increase the motion range drastically for these designs.

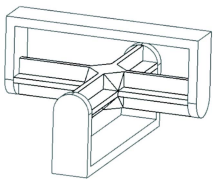

Figure 2.9: The CU joint with 2DOF [13]

Next to the stiffness being a problem for flexures at large displacements, there is another property that needs to be accounted for. The centre of rotation, defined by the intersection of the two lines coincident to the output linkages of the joint. For a rigid joint, the centre of rotation is strictly defined by the shape of the parts. For a flexure joint, this centre shifts with respect to its geometry. When looking again at the cross flexure hinge, this shift can be clearly seen in figure 2.10.

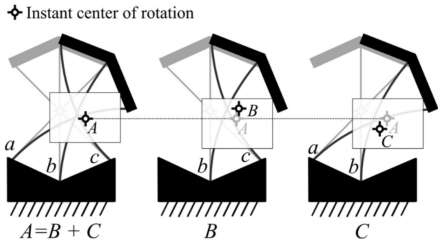

Figure 2.10: The calculated instant centre of rotation of a cross flexure hinge [12]

2.3.3 Flexible Delta Robots

Some research into Delta or parallel robots with flexible joints has been done. However, all of the research has been focused on either micro-robots or micro-assembly tasks. The flexible hinges are used because of their precision, not for the other advantages as stated in section 2.2. On top of that, most research on flexure joints is focused on revolute joints with high support stiffness. These joints could be used in a D2 robot, as is shown in figure 2.11, where a structure quite similar to a D2 delta robot has been build using only flexure joints. Due to the low support stiffness of the flexures at large deflections, the workspace of the robot is relatively small in comparison to the size of the robot. Even more so, if it is compared to a D2 robot with conventional joints of the same size.

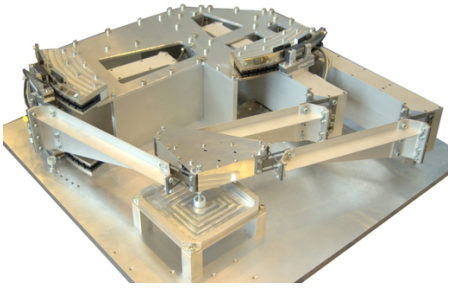

Figure 2.11: The large-stroke 2DoF flexure-based positioning stage for vacuum environments [14]

There has also been research into compliant delta robots with 3 DoF. The result of the research by Raatz (2003) [15] does create a macro delta robot and is the closest to the design goal set in this research, see figure 2.12b. The workspace of this robot is around 200x200x60 mm^3. Not quite large enough to be used in the pick and place industry, but a lot closer than the few millimetres that other flexible parallel robots can move. However, the focus of the robot is again micro-tasks. The hinges are designed to be very precise, but not very suitable for the problem at hand in the pick and place industry. They are very complex, not hygienic, and the motions of the ball joint are split up between two sets of hinges. This is something that is common between the different compliant delta robots. Probably due to the only available precision compliant hinges being revolute joints. This set of hinges can be clearly seen in figure 2.12b. Also note that in this robot, three linear actuators are used to actuate the secondary arms.

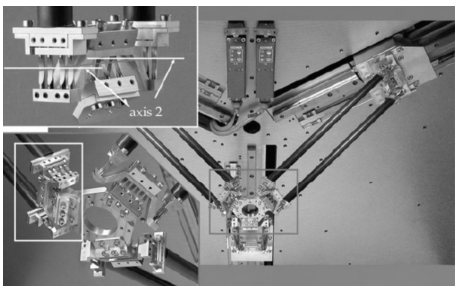

(a) An overview of the triglide robot.

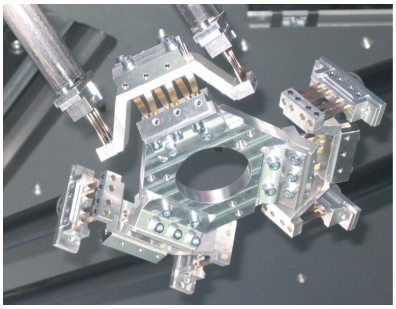

(b) A bottom view of the end effector

Figure 2.12: The compliant Triglide delta robot[15]

In the paper by Kozuka et al. (2013) bio-inspired joints are used as the building blocks for a flexible delta robot. With this precision robot, again, the two used DoF are split up over two revolute joints. This robot has a relatively large workspace for its size, with a workspace of 70x70x25 mm, but still nowhere close to the needed workspace for a pick and place robot. The hinges are also complex and difficult to clean.

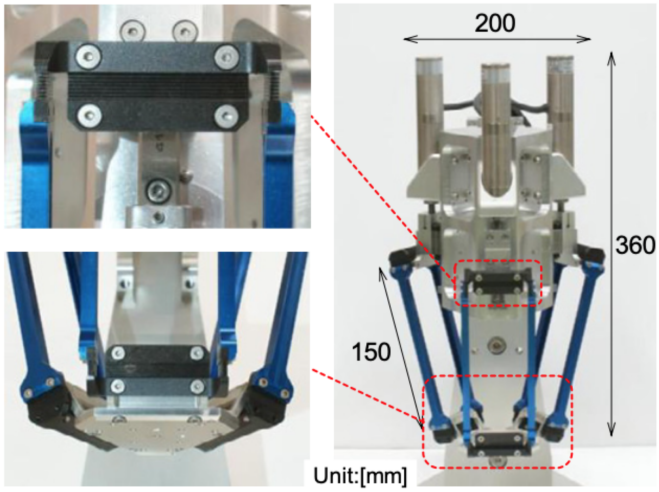

Figure 2.13: A bio inspired flexible delta robot[16]

Other versions of a fully compliant delta robot can be found, but only on a micro-scale. The milliDelta [17] is one of the latest examples, but some others can be found [18, 19, 20].

2.3.4 Materials

As all the flexures in the system will be used for millions of cycles, the material used has to be able to flex that many times as well. With steel, under a certain load, the material can be infinitely loaded, as can be seen in figure 2.14a. For polymers, this is a bit different, as there seems to be no infinite lifetime loading. This needs to be taken into account when designing the robot.

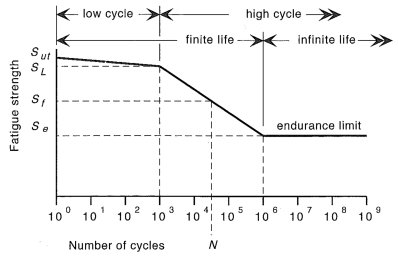

(a) A typical S-N diagram for steel [21]

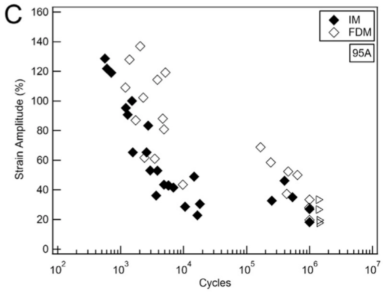

(b) Lifetime TPU 95A [22]

Figure 2.14: S-N diagrams for steel and plastic

For a full selection of available materials, CES Edupak is used. A good material for a compliant hinge should be able to elastically stretch a lot, to be able to deform to large angles. This means a high yield strength over a low Young's modulus. A representation of that can be seen in figure 2.15. From this, it is clearly visible why plastic would be a good material for a flexure hinge, as it has the highest ratio between yield strength and Young's modulus.

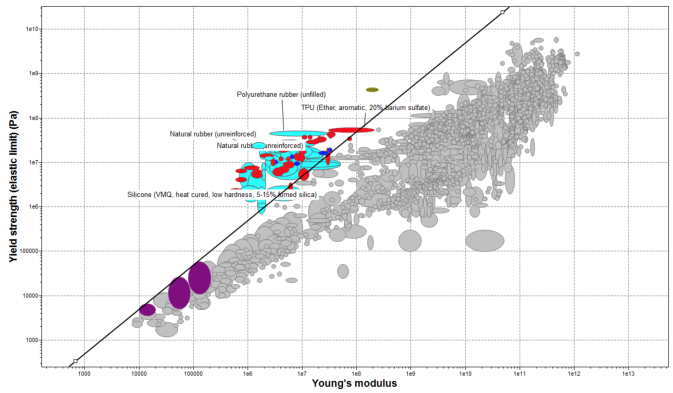

Figure 2.15: CES Edupak Ratio between Young's modulus and Yield strength

2.3.5 Overview of state of the art

Table 2.1: Overview

Paper	Workspace $[mm^3]$	Cleanability	Precision [mm]	Eigenfreq [Hz]	Operating Freq [Hz]	Payload [kg]	Lifetime
Triglide	200x200x60	low	1	120	-	-	-
Bio-Inspired	70x70x25	low	1	-	-	0.01	-
Millidelta	2x2x2	Medium	0.1	-	75	0.001	-
Requirements	1000x1000x400	High	1	60	2	2	10^7

From table 2.1, we can spot a clear gap in the literature so far. No large range delta robots that are hygienic have been researched yet.

2.4 Conclusion and Relevance

Although the structure and working principle of the Delta robot have been looked into and optimised, the joints used in the system can still be improved. The ball joints used for each of the parallelogram linkages have some disadvantages, especially when used in the food industry or dirty environments. Some research is done on compliant delta robots, but never with the focus on industrial pick and place actions. For this use case very high numbers of repetitions and a very large workspace are needed. This requires a completely new type of flexures, which can deflect to more than twice as much than 'large range flexures' found in literature while remaining high support stiffness. New materials and production techniques are looked at, as almost all research around flexures is based around the precision industry. This is one of the first times research has been done into using flexible couplings in the large scale production industry.

References

[1] *Bottle cap detection - Lanbao Sensing Technology Industrial Smart Sensor.*

[2] *KEBA - Bottle feeding delta robot - YouTube.*

[3] Ilian Bonev. *Delta Parallel Robot — the Story of Success.* Tech. rep.

[4] Raymond Clavel. *Device for the movement and positioning of an element in space.* 1989.

[5] *Nylatron® 703XL PA6 - Cast Nylon Engineering Material - MCAM.*

[6] *MURDOTEC 2000 G - Murdotec Kunststoffe.*

[7] Martin Wahle and Burkhard Corves. "Stiffness Analysis of Clavel's DELTA Robot". In: Springer, Berlin, Heidelberg, 2011, pp. 240–249.

[8] M.A. Laribi, L. Romdhane, and S. Zeghloul. "Analysis and dimensional synthesis of the DELTA robot for a prescribed workspace". In: *Mechanism and Machine Theory* 42.7 (July 2007), pp. 859–870. ISSN: 0094-114X.

[9] F. Pierrot et al. "High speed control of a parallel robot". In: *IEEE International Workshop on Intelligent Robots and Systems, Towards a New Frontier of Applications.* IEEE, pp. 949–954.

[10] Wei Dong, Zhijiang Du, and Lining Sun. "Stiffness influence atlases of a novel flexure hinge-based parallel mechanism with large workspace". In: *2005 IEEE/RSJ International Conference on Intelligent Robots and Systems.* IEEE, 2005, pp. 856–861. ISBN: 0-7803-8912-3.

[11] D. H. Wiersma et al. "Design and Performance Optimization of Large Stroke Spatial Flexures". In: *Journal of Computational and Nonlinear Dynamics* 9.1 (Jan. 2014). ISSN: 1555-1415.

[12] M. Naves, D. M. Brouwer, and R. G. K. M. Aarts. "Building Block-Based Spatial Topology Synthesis Method for Large-Stroke Flexure Hinges". In: *Journal of Mechanisms and Robotics* 9.4 (Aug. 2017). ISSN: 1942-4302.

[13] Brian P. Trease, Yong-Mo Moon, and Sridhar Kota. "Design of Large-Displacement Compliant Joints". In: *Journal of Mechanical Design* 127.4 (July 2005), p. 788. ISSN: 10500472.

[14] K. G. P. Folkersma et al. "A 2-DOF Large Stroke Flexure Based Positioning Mechanism". In: *Volume 4: 36th Mechanisms and Robotics Conference, Parts A and B.* American Society of Mechanical Engineers, Aug. 2012, pp. 221–228. ISBN: 978-0-7918-4503-5.

[15] Jürgen Hesselbach et al. "Design and Analyses of a Macro Parallel Robot with Flexure Hinges for Micro Assembly Tasks". In: 2003.

[16] Hiroaki Kozuka et al. "A compliant-parallel mechanism with bio-inspired compliant joints for high precision assembly robot". In: *Procedia CIRP*. 2013.

[17] Hayley McClintock et al. "The milliDelta: A high-bandwidth, high-precision, millimeter-scale Delta robot". In: *Science Robotics* 3.14 (Jan. 2018), eaar3018. ISSN: 2470-9476.

[18] Wei Dong, Zhijiang Du, and Lining Sun. "A large workspace macro/micro dual parallel mechanism with wide-range flexure hinges". In: *IEEE International Conference Mechatronics and Automation, 2005.* Vol. 3. IEEE, pp. 1592–1597. ISBN: 0-7803-9044-X.

[19] Dongwoo Kang and Daegab Gweon. *Analysis of large range rotational flexure in precision 6-DOF tripod robot.* 2012.

[20] Yuan Yun and Yangmin Li. "Optimal design of a 3-PUPU parallel robot with compliant hinges for micromanipulation in a cubic workspace". In: *Robotics and Computer-Integrated Manufacturing* 27.6 (Dec. 2011), pp. 977–985. ISSN: 0736-5845.

[21] Larry L. Howell. *Compliant mechanisms.* Wiley, 2001, p. 459. ISBN: 9780471384786.

[22] Andrew T. Miller et al. "Fatigue of injection molded and 3D printed polycarbonate urethane in solution". In: *Polymer* 108 (Jan. 2017), pp. 121–134. ISSN: 0032-3861.

Chapter 3

Paper: Modelling the axis drift of short wire flexures and increasing their support stiffness using polymers

Proceedings of the ASME XXXX International Design Engineering Technical Conferences & Computers and Information in Engineering Conference
IDETC/CIE XXXX
August XX-September XX, XXXX, San Diego, USA

DETCXXXX/MESA-XXXXX

MODELLING THE AXIS DRIFT OF SHORT WIRE FLEXURES AND INCREASING THEIR SUPPORT STIFFNESS USING POLYMERS

B. Daan
Dept. of Precision and Microsystems Engineering
Delft University of Technology
Delft, 2628 CD, The Netherlands
B.Daan@student.tudelft.nl

J. Rommers
J.L. Herder
Dept. of Precision and Microsystems Engineering
Delft University of Technology
Delft, 2628 CD, The Netherlands
J.Rommers@tudelft.nl - J.L.Herder@tudelft.nl

ABSTRACT

For steel flexures, complex geometries are required to reach high support stiffness and limit axis drift over large ranges of motion. These complex flexures are expensive and difficult to manufacture. This paper presents a method of designing short, polymer wire flexures with high support stiffness and modelling their axis drift using a novel method, the arc method. The arc method is validated against finite element methods (FEM) and physical tests, showing at least a factor 10 lower error than existing pseudo-rigid-body models (PRBM) at 70° *deflection, while maintaining a simple modelling approach. The use of polymers increases support stiffness of wire flexures by a factor 7800 with respect steel at* 70° *deflection, even though the material stiffness is substantially lower. This is due to the large allowed strain of polymers increasing the possible diameter by a factor 110.*

1 INTRODUCTION

The applications for compliant mechanisms range from the hinge of a shampoo bottle to the highest precision mechanisms. Flexures for precision applications are normally made from steel or other metals because of their predictability [1]. Flexures for consumer products are mostly made of polymer flexures, due to their ease of manufacturing. The use of polymer flexures in precision applications is still a mostly unresearched field, as polymers suffer from low repeatability and high creep. However, they allow for very large strain compared to steel.

With steel flexures, because of their low allowed strain, complex geometries are required to create high support stiffness over large ranges of motion [2]. But these complex flexures are expensive to manufacture and difficult to clean. Contrarily, as polymers allow for larger strain, using them for compliant joints allow thicker flexures for the same range of motion. This could result in high support stiffness over a large range of motion with simple geometries, such as the short wire flexure used as a two degree of freedom (2DOF) small-length flexural pivot.

A problem with simple flexures such as the short wire is that they exhibit axis drift when bending [3]. For rigid body joints, the rotation point or axis is defined by the shape of the joint and does not move when rotating. In more complex flexure designs, axis drift can be mitigated to some extent [4]. However, axis drift of a flexure has no influence on the repeatability of the flexure, but can have an effect on the accuracy of the system if the amount of axis drift is not known. The use of a feedback loop in the control system can correct for low accuracy to some extent, but a higher accuracy can then still decrease overshoot or settling time of the system [5]. To mitigate the accuracy loss due to axis drift, the feed-forward model of the system has to include this axis drift of the flexure when calculating the outputs of the system.

To model the axis drift of a compliant joint Pseudo Rigid Body Modelling (PRBM) or the Finite Element Method (FEM) is commonly used. In PRBM, flexure joints are replaced by revolute joints coupled with a torsional spring. PRBM does not model any axis drift and thus introduces an error [6]. As steel

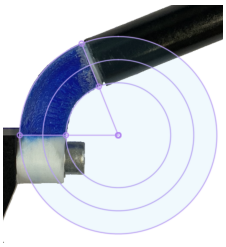

(a) A TPU Flexure bent to 70° showing circular deformation

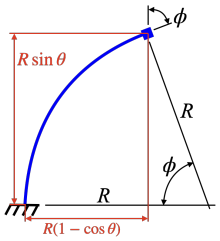

(b) A schematic drawing of arc method with the calculated endpoint positions

FIGURE 1: A TPU flexure and its arc method equivalent

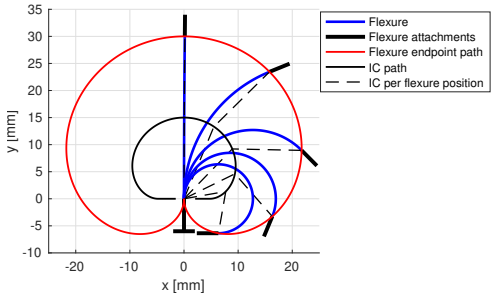

FIGURE 2: The endpoint path (red) of a flexure with a fixed arc length bending to $\pm 360°$, with some flexure positions drawn in blue. The IC path drawn in black, with dotted lines showing IC the position per flexure position.

wire flexures are mostly implemented for small deflection angles, where the effect of axis drift is small, PRBM could still offer high enough accuracy. However, if polymer flexures such as researched in this paper allow for a large range of motion, the error of PRBM increases. Multiple revolute joints per flexure instead of one reduces the error but increases complexity. Howell proposes a solution for this, an optimised single revolute joint position per loading condition, called the characteristic pivot [1]. For this method, however, the loading condition needs to be known, and an angle error is introduced at the endpoint of the flexure. FEM simulates the deflection of a flexure accurately, but a separate simulation for each flexure and bend angle would be required, resulting in large lookup tables, quickly increasing complexity. A simple analytic model for wire flexures for a large range of motion is not yet available.

This paper aims to develop a simple analytic model to accurately model the axis drift of wire flexures used as 2DOF small-length flexural pivots for a large range of motion. To increase robustness and precision of the flexure, the use of polymers for the design of wire flexures with high support stiffness for this large range of motion is investigated.

The structure of this paper is as follows. In section 2, an analytic model named arc method is developed for the axis drift of wire flexures. In section 3, the support stiffness and differences between a steel and polymer wire flexure are investigated. In section 4, the results for both of these methods are presented, after which they are discussed in section 5. Finally, conclusions are presented in section 6.

2 THE ARC METHOD

In section 2.1 a new simple way of modelling wire flexures is proposed, the arc method, after which a technique for implementing this method into kinematic models is given in section 2.2. Finally, it is compared to existing PRBM in section 2.3.

2.1 Modelling Axis Drift With The Arc Method

The arc method uses three theories for cantilever beams to model wire flexures. First, if a cantilever beam is bent by a moment on its free endpoint, the shape of the flexure follows a circular arc, as both the moment and area moment of inertia is constant over the length of the flexure. Second, the neutral axis, which is the axis that does not see any strain or longitudinal forces during bending, does not change length. Third, as the cross-section of a wire flexure is symmetric, the neutral axis lies in the centre of the flexure. Thus, a wire flexure of length L bent by a moment to an angle ϕ can be modelled by a circular arc at its centre line with a constant length L and an angle ϕ. This modelling approach we call the arc method. Figure 1a shows a bent wire flexure made from thermoplastic polyurethane (TPU), and its arc method equivalent in figure 1b. Based on the radius of curvature, which for an arc of known length is specified by $R = \frac{L}{\phi}$, the positions of the endpoint of an arc can easily be found, as also shown in figure 1b.

Any external force deviates the flexure from this arc, as this introduces compression, shear, and an unequal bending moment over the length of the flexure. A high support stiffness can decrease this effect, as will be investigated in section 3. External forces will not be taken into account in this section.

Figure 2 shows the path of the endpoint of the flexure for different deformation angles calculated with the arc method. Also drawn in this figure is the centrode, or path of the instant centre of rotation (IC) of this flexure. The IC is the point around which the rigid body connected to the flexure pivots at each instant. The IC must lie on the line perpendicular to the midpoint of the flexure, as the flexure is symmetrical around this line. The IC can then be determined by intersecting a line perpendicular to the velocity vector of the endpoint with this middle line. The path of the endpoint is known, and the velocity vector must always lie tangent to the path. The migrating IC shows the axis drift of the flexure.

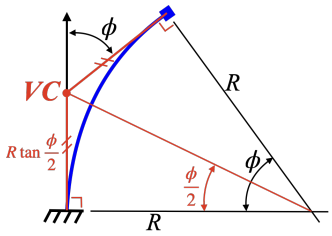

FIGURE 3: The definition of the virtual centre (VC) for a bent flexure. This definition works both in 2D, as depicted here, and in 3D. The VC always lies along the vector tangent to the base of the flexure, depicted in this figure by the black arrow pointed upwards.

2.2 Using The Arc Method For Kinematic Models

With an arc of known length in between each of the rigid bodies, the kinematic model is fully defined and can thus be solved. This means the kinematics of a complex, multi-flexure system can be accurately modelled. To make this method easier to implement, a virtual centre (VC) can be added to the system. This centre is an intersection of the two tangent lines to each of endpoints of the flexures, as can be seen in figure 3. It is important to note that this is not the same as the IC of the flexure, which can be seen in figure 2. Using this VC to solve the system changes the multi flexure model back into a more PRBM like system, but implementing shifting rotation pivots. Two things make this VC well suited for solving the system in comparison to working with the arc method directly or using the IC. First, the VC shifts along a single vector for every deflection angle, as it always lies on the tangent at the base of the flexure. Second, the point is easily calculated based on the deflection angle ϕ of the flexure. Looking again at figure 3, the distance between the base of the flexure and the VC is defined as $R \cdot \tan \frac{\phi}{2}$.

A drawback of using the arc method and VC however, is that due to the shifting rotation pivots the distance between the pivots is dependent on the deflection angle. This increased complexity can result in a necessity for an iterative solver in some systems.

2.3 Comparing The Arc Method To PRBM

For PRBM methods with a single rotation pivot, three methods are found in literature. One has the pivot at the base of the flexure, one centred on the flexure, one at a characteristic pivot location based on the loading condition. Each draws a different circle for the endpoint of the flexure, which are all depicted in figure 4. To find the characteristic pivot, Howell matches the path of the endpoint per loading condition to a circle to minimise the error [1]. For a flexure with an applied moment, a circle with a radius of 0.7346 matches the path best. To then match the deflection rate, an angle coefficient is used, in this case 1.5164. This means that for a flexure angle of 1.5164° degrees,

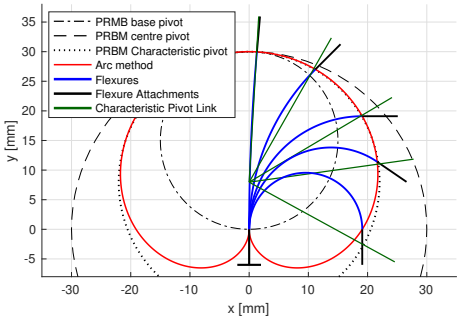

FIGURE 4: The comparison between the arc method and three PRBM approximations. One with the pivot at the base of the flexure, one at the centre of the flexure and one at the characteristic pivot. Flexure shapes for different deflection angles are also shown in blue, as well as the characteristic pivot with angle coefficient in green. The angles for these are: 5°, 45°, 90°, 124.4°, and 180°. 124.4° is the maximum angle for which Howell specifies a position error of less then 0.5% of the tip deflection.

the PRBM linkage has an angle of 1°. Figure 4 shows the green lines modelled by the characteristic pivot with angle coefficient almost intersecting the endpoints of the flexure modelled by the arc method. However, the approximations necessary for the characteristic pivot add complexity compared to the arc method. Next to this, as the arc method describes the exact way a wire flexure deforms due to a moment, the characteristic pivot is also less accurate. The drawbacks of the characteristic pivot only increase when the body connected to the flexure has to be modelled, as the angle coefficient creates an angle error at the endpoint of the flexure. This error can also be seen in figure 4, where the actual flexure attachment in black has a different angle than the characteristic pivot link in green.

3 SUPPORT STIFFNESS

Deflections caused by external forces can cause an error in the prediction of the arc method. A high support stiffness decreases this error, increasing the robustness of the model. In section 3.1, the support stiffness for a short wire flexure is defined, after which the effect of material strain is investigated in section 3.2. The support stiffness is then modelled in section 3.3.

3.1 Defining Support Stiffness For A Wire Flexure

For a short wire flexure used as a 2DOF small-length flexural pivot, we define the support stiffness to be the following: The stiffness against loading at the endpoint tangent to the flexure while constraining its rotation, as is illustrated in figure 5. This is based on the loading of a ball joint in its most common use, a truss-like setup where a rod has a ball joint at either end, resulting

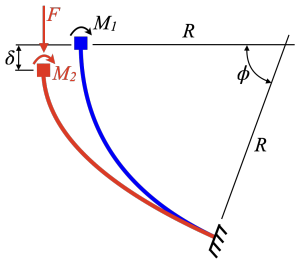

FIGURE 5: Support stiffness F/δ of a bend short wire flexure, where ϕ is the deflection angle of the flexure. Moment M_1 is the bending moment necessary for this deflection angle. Moment M_2 consists of the initial bending moment plus the constraining moment to keep the angle ϕ when loading.

in a two force member. The rod can only be in pure compression or tension, but the mechanism does input a certain deflection angle on the ball joints. In such a system, the distance between the two joints constrains the mechanism, so the deflection in this direction, in line with the loading force, is investigated.

The loading force introduces three kinds of deformation types in the flexure: compression, shear, and bending. Due to these deformations, the deflection angle of the flexure changes. This is not allowed, as the rotation of the endpoint of the flexure is constrained by the attached system. This constraint results in an additional moment at the endpoint of the flexure. For each of these deformation types, linear beam theory prescribes an equation for its stiffness. These equations show that the support stiffness is dependent on the diameter, length, material stiffness, and Poison's ratio. However, the maximum strain a material allows also indirectly influences the support stiffness, as it defines the ratio between thickness and length of the flexure for a given range of motion.

3.2 Influence Of Strain On Flexure Geometry

The amount of strain in a flexure is dependent on the length, thickness, and deflection angle of a flexure. For a bent flexure as can be seen in figure 6, the following can be found. A thicker flexure of the same length increases strain, as both the stress and strain increases linearly away from the neutral axis of the flexure. Contrarily, a longer flexure decreases strain, as the bend is spread out over a longer distance. Therefore the length over radius ratio of the flexure L/r is investigated, and how the amount of strain that is allowed in a material limits this ratio.

When bending a flexure, the outer sides have the highest amount of strain. The neutral axis for the wire flexure, which is the axis which does not see any strain or longitudinal forces during bending, lies in the centre of the flexure. This neutral axis then also does not change in length during bending. From this, the strain in the material at the outer sides can be found by

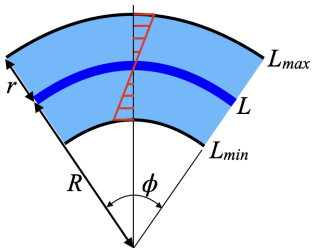

FIGURE 6: A bend wire flexure to angle ϕ. The undeformed length of the flexure is L, which is still the case at the centreline. The elongated outside of the flexure has an length of L_{max}, while the compressed inside has a length of L_{min}. The radius of curvature is R, and the radius of the flexure itself is r.

rewriting the formula for strain:

$$\varepsilon_{max} = \frac{dL_{max}}{L} = \frac{L_{max} - L}{L} \tag{1}$$

As the flexure forms a circular arc, the arc length of a flexure is equal to $L_{arc} = R\phi$. The L_{max} of the flexure can be rewritten as:

$$L_{max} = \phi(R + r) = L + r\phi \tag{2}$$

Filling this into the equation 1 gives:

$$\varepsilon_{max} = \frac{L + r\phi - L}{L} = \frac{r\phi}{L} \tag{3}$$

We define the maximum allowed strain as the maximum strain before yielding. This maximum strain is given by $\varepsilon_{allowed} = YS/E$. In literature, this strain is also called elongation at yield, or elasticity percentage. Combining this maximum strain with equation 3 results in equation 4. In this equation, only strain by bending is taken into account. External forces can cause additional strain in the flexure, requiring either a thinner or longer flexure. As this is dependent on the use case of the flexure, it is not taken into account here.

$$\frac{L}{r} = \frac{\phi_{max}}{\varepsilon_{allowed}} \tag{4}$$

From equation 4 it can be seen that for a certain deflection angle of the flexure, a material with a higher maximum strain allows a larger diameter for the same length. This means that materials that allow more strain but have a lower young's modulus can still result in a higher support stiffness. To test this theory, a material that allows one of the highest amount of strain is looked at, polyurethane [7]. Polyurethane can stretch up to 100% without yielding, while for steel this is only about 0.5%. For the tests in this paper, a 3D printable TPU is used with a maximum strain of 55% [8], still a factor 110 larger than steel. This results in a wire flexure with a diameter that is also 110 times larger, or D_{ratio} = 110. However, the Young's modulus of TPU is a lot

TABLE 1: Stiffness ratio of steel over TPU for each deformation mode based on linear beam theory, showing the stiffer TPU, especially in bending. D_{ratio} and E_{ratio} are the ratio between two materials' diameter and Young's modulus, respectively

Deformation mode	Stiffness ratio equation	$\frac{TPU}{Steel}$
Compression	$D_{ratio}^2 \cdot E_{ratio}$	1.6
Shear	$D_{ratio}^2 \cdot E_{ratio} \cdot \frac{1+\nu_1}{1+\nu_2}$	1.7
Bending	$D_{ratio}^4 \cdot E_{ratio}$	1.9×10^4

lower than steel, 26 MPa vs 200 GPa, respectively. This difference is approximately a ratio of $E_{ratio} = 1.3 \times 10^{-4}$. Finally, the Poisson's ratio of steel is 0.28 and for TPU 0.4. The stiffness differences for each deformation mode can now be calculated based on the equations from linear beam theory, as is shown in table 1. TPU is stiffer in each deformation mode, which results in a higher total support stiffness of the flexure. How much higher exactly is based on how each deformation mode influences the total support stiffness of the flexure, as especially bending stiffness is higher for TPU. To find the ratio between each of the deformation modes, and how they change for different deformation angles, a model is made for the support stiffness of the wire flexure.

3.3 Modelling Support Stiffness

A model for the support stiffness could be based on testing in a tensile testing machine or modelling in a FEM program. However, to create an understanding for how much a certain parameter influences the support stiffness, many parameter studies would need to be performed. Instead, a model is created based on linear beam theory, which can then be checked against FEM programs. As stated in section 3.1, the force introduces compression, shear and bending on the flexure. The contribution to the support stiffness of each of the deformation types changes for different deflection angles of the flexure. For very small deflection angles, the force almost solely introduces compression in the flexure and thus the support stiffness will be dominated by the compression stiffness, or limited by buckling. For large deflection angles, compression in the flexure decreases while bending and shear increase. If the ratio between each of these aspects is known, also the effect of each design parameter on the support stiffness can be determined. This can be taken into account to optimise flexure designs for high support stiffness.

To calculate these ratios, a finite element model is made. The difference with a simulation in a FEM program is that the model in this paper is specific to the calculation of support stiffness, giving both more control and showing in more detail the effect of each parameter on the support stiffness. The wire flexure is split up in small elements along the flexure of size $d\theta$, and

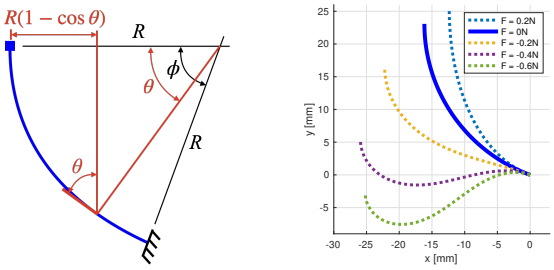

(a) The moment arm $R*(1-\cos\theta)$ and angle θ of the loading force on an element along the bend flexure.

(b) Different loading forces on a bend steel flexure with a length of 30 mm and diameter of 0.25 mm, bent to 70°.

FIGURE 7: Support stiffness modelling approach

for each, the deflection from each contribution is calculated. In this model, each element is approximated as a circular arc, similar to Chen [9]. The amount of each deformation type changes along the flexure. At the tip, the force is in line with the flexure, resulting in pure compression. From figure 7a it can be seen that at the base, the force has both an angle ϕ and a moment arm of $R*(1-\cos\phi)$, increasing deflection from shear and bending but decreasing from compression. Any point in between at angle θ has the force at this angle θ and a moment arm of $R*(1-\cos\theta)$.

Each deformation type has a different effect on a small element. Compression changes the arc length of the element. Shear shifts two elements with respect to each other. Shear is modelled by rotating each element by its shear angle γ. The moment caused by the force is added to the already existent bending moment in each element, changing the radius of curvature. It is not taken into account yet, that the deflection angle is constrained by the attached system. This adds an additional moment on the flexure as is shown in figure 5. As only bending causes a change in rotation of the flexure, the bending moment in each element can be integrated over the length of the flexure, and added to the endpoint of the flexure. To increase accuracy for large deformations, the model can be looped to include the effect of deflection increasing the moment arm in the flexure, which in turn increases deflection, as shown in figure 7b.

From this model can indeed be seen that the effect of compression decreases while bending and shear increase. This is true for every flexure, as it is coupled to how the force interacts with the flexure, not the wire flexure geometry or material. However, the ratio between compression, shear and bending do change with different geometry or material constants, and so does the total support stiffness of the flexure. The results for a TPU and steel flexure are given in section 4.2

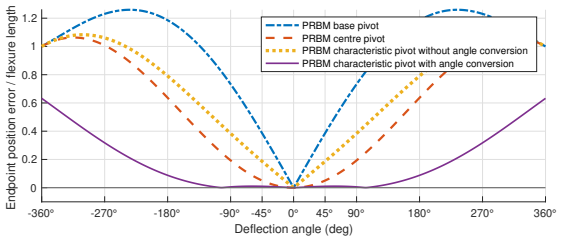

FIGURE 8: The normalised error of endpoint calculated by the different PRBM methods against the actual flexure deformation calculated with the arc method plotted over the deformation angle. The PRBM methods without an angle coefficient all have an error of 1 at 360°, meaning a full flexure length of error. This is because the arc method correctly predicts that the flexure shape creates a loop at 360° deflection, having the endpoint and base of the flexure touch, while the circle paths of the PRBM methods rotate back to their starting position. Hence, a flexure length of error.

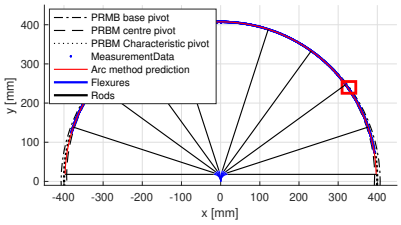

FIGURE 9: The position of the endpoint of a rod attached to a 3D printed TPU flexure, with a few flexure and rod positions drawn in. The flexures are drawn in blue at the bottom centre of the figure, with the black rods extending from the flexures. Also drawn are the PRBM paths for each of the three rotation points. The flexure is made from TPU, has a diameter of 15 mm and a length of 25 mm. The rod has a length of 380 mm. A zoomed in view of the red rectangle is given in figure 10

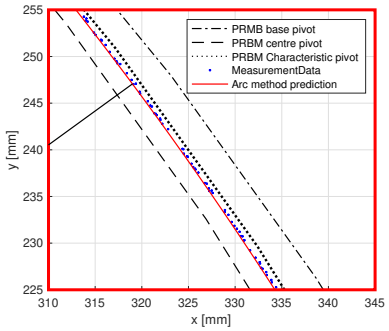

FIGURE 10: A zoomed in section from the red rectangle from figure 9. Here the difference between the path of the three PRBM methods and that of the arc method with respect to the measurement data can be seen.

4 RESULTS

In section 2 and 3, two models are developed for the short wire flexure, for which the results are presented in this section. The first model shows the axis drift and flexure shape of the short wire flexure, of which the results are given in section 4.1. The model is compared against PRBM, and checked against a FEM program. Finally, the method is measured against a physical test by deflecting a polyurethane wire flexure whilst measuring its position and rotation. The second model shows the support stiffness and the effects of different flexure parameters on this stiffness. The results of this model are given in section 4.2. The model is then checked by comparing the total support stiffness to results from FEM programs.

4.1 Arc Method Results

The results of the arc model are checked against data from COMSOL Multiphysics®. Both the 2D beam mechanics and the 3D solid mechanics interfaces are used. If a moment is placed on a beam in the beam mechanics interface, the path of the endpoint matches within 0.01% with the arc method over a deflection of 360°. The path for the 3D model of the steel flexure matches within 0.1%. The 3D model of a TPU Flexure matches closely for small deformations, but the error increases as the deflection angle increases. For a deformation angle of 50°, the error is 1.9%.

In figure 8, the error of each of the PRBM methods with respect to the arc method is calculated. Three PRBM methods are compared, each with a different pivot location. These PRBM methods can also be seen in figure 4. The error is calculated by taking the distance between the endpoint of each method for a given deflection angle. Figure 8 also shows that when the characteristic pivot PRBM is used with the angle coefficient, high accuracy for modelling the endpoint is reached for angles up to 124.4°. Do note that this accuracy is for the endpoint of the flexure, as the angle coefficient introduces an error for the attached system as discussed in section 2.3. If the angle coefficient is not used, the error is higher than that of the PRBM approximation with centre pivot.

The arc method is tested against measurements done on a TPU flexure hinge such as in figure 1a. Here the endpoint position of a rod attached to the TPU Flexure is measured over a large deflection range of $\pm 70°$ as is shown in figure 9. In this figure, the test data is shown, as well as the PRBM and arc method. A zoomed-in view of this data can be found in figure 10, where the differences between the methods can be seen in more detail.

The error of the measured data with respect to the arc method is shown in figure 11. The maximum error is found at the largest deformation angles, ≈ 0.4 mm error at $\pm 70°$. The trend

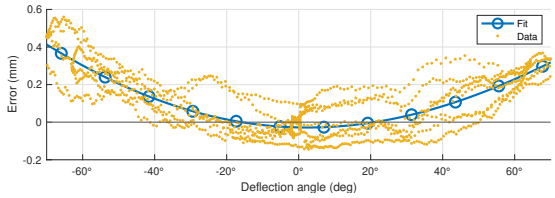

FIGURE 11: Error of the tested data to the arc method predictions. A positive error means the measurement data lies outside of the arc method. The smoothing spline fit shows a maximum error of 0.4 mm at 70°

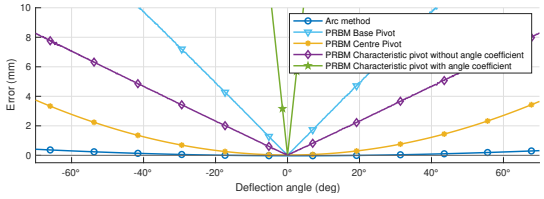

FIGURE 12: The error of the PRBM and arc method. At 70°, the arc method shows a factor 10 lower error than most accurate PRMB, which is the centre pivot PRBM. The characteristic pivot performs worse even though the path seems to match better, as the angle is also taken into account. Each of the lines is a fitted average of the data using a smooth spine fit. PRBM base pivot and Characteristic pivot with angle conversion continue linearly to $\pm 70°$.

of the data shows however a drift in this error. While the arc method matches for small angles, for large angles the measured data is outside of the arc method prediction. However, to put this error into perspective, it is compared against the error of the different PRBM. The results of this comparison can be found in figure 12. The smallest error of a PRBM method at these $\pm 70°$ is ≈ 4 mm, a factor 10 more. The PRBM method with characteristic pivot shows larger error than the centred PRBM, even though the path seems to match better as can be seen in figure 10, as the deflection is also taken into account when calculating the error.

4.2 Support Stiffness Results

The support stiffness model from section 3.3 is used to model the stiffness of a steel flexure and a TPU flexure over a range of bend angles, as shown in figure 13.

Figure 13 also shows how at an deflection angle of 0° the ratio between the support stiffness is 1.6, comparable to the difference in pure compression stiffness as stated in table 1. At large deformation angles, this ratio quickly increases, to approximately 7800 at 70°. To see what parameters affect this stiffness, the contribution of each deformation type to the total compliance of the flexure is investigated, which can be seen in figure 14.

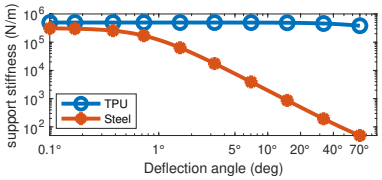

FIGURE 13: The support stiffness of a steel and TPU wire flexure for different bend angles. From an angle of 1°, the support stiffness of the steel flexure drops, until a ratio of 7800 at 70°. Each has a diameter that corresponds to a length of 30 mm and a maximum bend angle of 70°. For steel this is a diameter of 0.25 mm, for TPU it is 27 mm

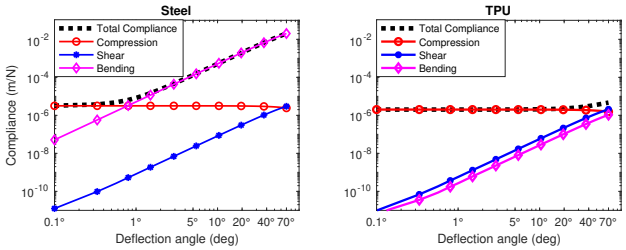

FIGURE 14: The contribution of compression, shear and bending to the total compliance for a steel and TPU Flexure, plotted for different deflection angles. The compliance of the steel flexure increases due to the low bending stiffness to 10^{-2} at 70° The compliance of the TPU flexure stays at 10^{-6}.

Do note that figure 13 and 14 only show the instant support stiffness calculated by the support stiffness model, not taking into account the non-linear loading behaviour of the flexure. Especially with the thin steel flexure, this behaviour causes a decrease in stiffness when the flexure is compressed. When the loading force deforms the flexure, the moment arm of this force is increased, which then increases deformation again. This behaviour is seen in figure 15.

The results of the support stiffness model are checked against data from COMSOL MultiPhysics®. Both the 2D beam mechanics and the 3D solid mechanics interfaces are used. The models match within 0.1% with the data from the beam interface for both TPU and steel, for a large deflection range as shown in figure 15. The 3D steel flexure also matches with the support stiffness model. However, the deflection results from the TPU flexure in the solid mechanics interface do deviate from the support stiffness model at large deflections. The instant stiffness does match within 0.1%, but as soon as the flexure starts deforming, the error increases. This error ranges from 1% at a compression force of 10 N giving a deflection of 0.1 mm, to 14% at 100 N giving a deflection of 1.2 mm.

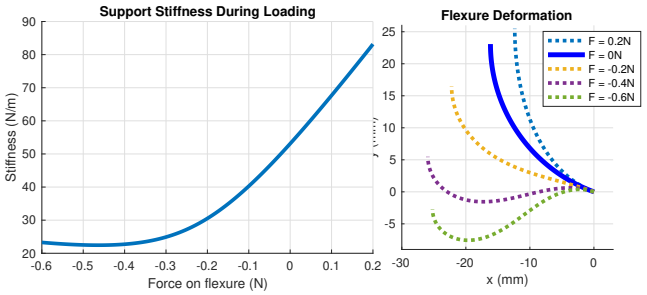

FIGURE 15: The support stiffness behaviour of a steel wire flexure during loading. On the left, the drop in stiffness for higher loading forces, caused by the increased moment arm which is shown the right.

5 DISCUSSION

5.1 The Arc Method

The measurement results show the arc method has higher accuracy than the existing PRBM methods. However, figure 11 shows a mismatch between the predicted path by the arc method and that of the flexure. At large deflections especially, the data lies outside of the predicted curve by the arc method. For this to happen, the flexure either has to increase in arc length or not follow a circular arc. It is not likely that the flexure deviates from the circular arc, as the bending moment, shape, and material are the same over the length of the flexure. That means that the flexure increases in arc length, thus elongates while deforming. This could be caused by a difference in compression vs tension behaviour in the flexure. If the TPU used for the flexure is stiffer in compression than it is in tension, a bending moment will cause the flexure to elongate. A difference in creep or hysteresis between tension and compression could also be the cause, as this gives the same effect as the difference in stiffness. The flexure for the tests was 3D printed, which could also further introduce non-linear material effects.

The measurement results also show the effect of the endpoint angle error introduced by the angle coefficient for the characteristic pivot. This method only works up to the endpoint of the flexure, not taking into account any systems that attach to it. An additional bend could be added to the endpoint of the flexure, bending back to the original angle. However, this increases complexity, as the distance between the PRBM pivots is now not constant anymore, but changes for different deflection angles. Just as with the arc method and VC, this can result in a necessity for an iterative solver when solving a system with multiple flexures. Another possible option is to match the angle coefficient and characteristic pivot not for the flexure itself, but for the flexure and attached rod together. This could work for a single joint, but in systems with multiple joints this also increases complexity. Based on this, two options arise for modelling flexure systems. Of the less complex methods with a fixed single pivot, the PRBM model with a centre pivot has the lowest error. If high accuracy is required, the arc method has a tenth of the error of PRBM, but a higher complexity due to the shifting pivot location.

5.2 Support Stiffness

The support stiffness model shows a large increase in support stiffness for the TPU flexure with respect to the steel flexure, mainly because of the large increase in bending stiffness for the TPU flexure. The deformation of the steel flexure is quickly dominated by deformation due to bending. For the TPU flexure, due to the larger diameter and thus high area moment of inertia, the contribution to the deflection of compression and shear are larger than that of bending.

The support stiffness model overall matches the results from COMSOL Multiphysics® closely, only for large deflections of the TPU flexure the error increases. This is likely caused by the behaviour of the flexure at the attachment points and effects like anticlastic curvature, which are not taken into account in the support stiffness model, but are modelled in COMSOL Multiphysics®.

5.3 Applications Of The Methods

Both the support stiffness model and arc method are now focused on the short wire flexure, but are not limited to only that application. Using high strain materials such as polymers to increase support stiffness can be applied to other flexure types, as each of the deformation types is stiffer for TPU with respect to that of steel. The exact increase in support stiffness is dependent on the application, as the bending mode shows the largest stiffness difference.

5.4 Material Assumptions

The TPU used in this paper was assumed to be a homogeneous material with linear material behaviour. Polymers also suffer from high creep, which also was not taken into account in this paper. The test samples used in this paper were 3D printed, limiting the quality of material possible. Using injection moulding could result in higher yield over Young's modulus, resulting in shorter and thicker flexures, giving even higher stiffness. Polymers have higher internal friction than steel, which combined with the larger strain could result in heating of the flexures, changing material constants. This large internal friction can also act as internal damping, reducing the vibrations in the system. Next to this, flexures from combinations of different materials such as a steel core and polymer outside could even further increase precision and accuracy of flexure systems.

6 CONCLUSION

This paper presents a simple analytic model for the axis drift of wire flexures for large ranges of motion. This model, named the arc method, models the flexure as a circular arc, based on the deformation by a pure moment. A virtual centre is defined to more efficiently include the arc method in kinematic models, as it simplifies the system to a single rotation point per deflection angle of the flexure.

The arc method is validated by comparing it to FEM and a physical test, both showing good agreement. Different PRBM methods are also compared against the measurement data, showing a factor 10 larger errors than the arc method at deflections of 70°.

Next to this, this paper shows how the use of polymers can increase precision and robustness of a short wire flexure. The diameter of a flexure is defined by the maximum allowed strain and required deflection angle. Based on this, the large allowed strain of polymers results in a larger diameter than steel for the same bend angle.

The support stiffness model from this paper shows how polymers increases support stiffness even though the material stiffness is substantially lower than that of steel. This model also shows the influence of the different deformation types on the support stiffness of a bent flexure. This gives the possibility to increase support stiffness by optimising the stiffness of each deformation type.

The support stiffness model is validated by comparing it to FEM showing a maximum error of 0.1% to the 2D beam interface, and a matching instant stiffness for the 3D solid mechanics interface.

To conclude, combining high support stiffness from polymers with the arc method can result in flexures with high precision and accuracy while having a simple geometry such as a wire flexure.

REFERENCES

[1] Larry L. Howell. *Compliant mechanisms*. Wiley, 2001.

[2] M. Naves, D. M. Brouwer, and R. G. K. M. Aarts. Building Block-Based Spatial Topology Synthesis Method for Large-Stroke Flexure Hinges. *Journal of Mechanisms and Robotics*, 9(4), 8 2017.

[3] D. Farhadi Machekposhti, N. Tolou, and J. L. Herder. A Review on Compliant Joints and Rigid-Body Constant Velocity Universal Joints Toward the Design of Compliant Homokinetic Couplings. *Journal of Mechanical Design*, 137(3), 3 2015.

[4] Brian P. Trease, Yong-Mo Moon, and Sridhar Kota. Design of Large-Displacement Compliant Joints. *Journal of Mechanical Design*, 127(4):788, 7 2005.

[5] I. Gustavsson, L. Ljung, and T. Söderström. Identification of processes in closed loop—identifiability and accuracy aspects. *Automatica*, 13(1):59–75, 1 1977.

[6] Zhonglei Feng, Yueqing Yu, and Wenjing Wang. Modeling of large-deflection links for compliant mechanisms.

[7] GRANTA EduPack — Granta Design.

[8] Ultimaker TPU 95A material: 3D print durable and flexible parts.

[9] Guimin Chen, Fulei Ma, Guangbo Hao, and Weidong Zhu. Modeling Large Deflections of Initially Curved Beams in Compliant Mechanisms Using Chained Beam-Constraint-Model. 2018.

Chapter 4

Discussion

The flexures developed for the delta robot in this thesis are based on the results of the paper in section 3. In the paper, the advantages of the TPU flexures and arc method have already been discussed. This discussion is on the implementation of these flexures on the delta robot, and the other research presented in the appendices. First, a short discussion on each appendix is presented in section 4.1. Next, the advantages of the developed delta robot with flexure hinges is discussed in section 4.2. Finally, other research opportunities are given in section 4.3.

4.1 Discussion of Appendices

In appendix A, the PRBM with characteristic pivot and angle coefficient is checked against the arc method. An additional bend is proposed to increase accuracy when modelling the attached body. However, even with the additional bend, the accuracy is still lower than that of the arc method, and the complexity higher.

Appendix B shows the flexure design process, implementation and testing on the delta robot. The flexures show high performance, with the maximum reached pick and place speeds go from 200 with ball joints to over 400 picks per minute over a path of 600 mm. Next to this, the arc method has been implemented on the full inverse kinematic model of the delta robot, as is shown in appendix C. The measurements done with this feed-forward model show a maximum error of 0.01° on the motor input angles, comparable to the precision of motor drivers.

In appendix D, a conceptual design for a compliant rotation shaft for a delta robot is presented. This concept replaces both the U-joint and linear bearing in the additional centre shaft of a delta robot, which is used to input a rotation on the end effector. The initial prototypes show how the new type of flexure joint could be used in a delta robot.

Finally, in appendix E, the test setups are shown that are used for the validation of the models presented in the paper. A delta robot was used to test the accuracy of the arc method and a tensile test the support stiffness. However, the tensile test results could not be used in the paper due to a low accuracy of the machine.

4.2 Advantages of the Developed System

- *Mass* - The flexure replaces the ball joint assembly, which consists of a metal ball, nylon cup, POM rod attachments, and spring assembly. The flexure is only a fraction of the weight of all these components, only 10 g versus 70 g. Each delta robot comprises of 12 ball and socket joints, so the overall weight savings are significant at 720 g. This directly influences the speed of the robot, due to the lower inertia of the system.
- *Hygiene* - Due to the monolithic design of flexure joints, the amount of creases is reduced in the system, resulting in fewer places for dirt and bacteria to accumulate. It also makes the robot easier to clean, also increasing hygiene.
- *Cost* - Due to the simple design of the flexure and fewer parts, the production cost is low. Not only with respect to other flexure solutions, but especially also with respect to the ball and socket joint.
- *Lifetime* - As there are no friction surfaces in a flexure joint, no wear and thus unlimited lifetime could be possible.
- *Maintenance* - Flexure joints do not require lubrication or other maintenance, resulting in less downtime of the system.

4.3 Research Opportunities

- *Material Study* - The current version 3D printed TPU flexure is tested on the delta robot, mainly to test their endurance. Some different types of polymers were tested, but an in-depth material study on the different types of polymers and their advantage could still improve the performance of the system.
- *Effect of material creep and hysteresis on flexure performance* - Polymers suffer from large creep and hysteresis with respect to steel, which can have a negative effect on the performance of the flexure. A study on how large this effect is and how it can be reduced would further improve the accuracy of the system.
- *Using internal friction for system damping* - As polymers have high internal friction, they dampen out motions by converting motion energy to heat. Using the TPU flexures on the delta robot, the flexures warmed up slightly, but quickly reached steady state. This effect of internal damping could be used to reduce eigenmode excitation in the system.
- *Application of methods* - Both the support stiffness model and arc method are now focused on the short wire flexure, but are not limited to only that application. Using high strain materials such as polymers to increase support stiffness can be applied to other flexure types, as each of the deformation types is stiffer for TPU with respect to that of steel. The exact increase in support stiffness is dependent on the application, as the bending mode shows the largest stiffness difference.
- *Compliant rotation Arm* - The conceptual design for the compliant rotation arm already shows potential and could be further explored.

Chapter 5

Conclusion

The objective for this thesis was to develop a flexure hinge to replace the ball joints of a delta robot from Codian Robotics. These flexures require high support stiffness over a large range of motion, have to be feed-forward modelled, and also be hygienic. The literature research shows how current flexures are not suited for this application. However, using other materials than steel for flexure hinges such as polymers could result in flexures that meed the requirements.

The paper from chapter 3 develops a new method, the arc method, to feed-forward predict simple wire flexures, and how the use of polymers increases their support stiffness. Based on a physical test, the arc method was shown to have at least a factor 10 lower error than the best PRBM approximation. A model for the support stiffness of wire flexures is developed, where the difference between a TPU and steel flexure is investigated. This results in a factor 7800 higher stiffness for the TPU flexure at 70°.

A TPU flexure is designed based on the research from the paper and is implemented in the delta robot. Initial tests show that the flexure system can already reach twice as high speeds as the conventional delta robot and has been tested half million pick and place cycles. The delta robot with flexures is 720 g lighter, has fewer creases and pockets, and has lower production and assembly costs.

Appendix A

Increasing Accuracy PRBM with Characteristic Pivot

The PRBM with the characteristic pivot and angle coefficient model the position of the endpoint within an error of less than 0.5% for angles up to 124.4°. However, it introduces an angle error when using it to model more than the endpoint of the flexure.

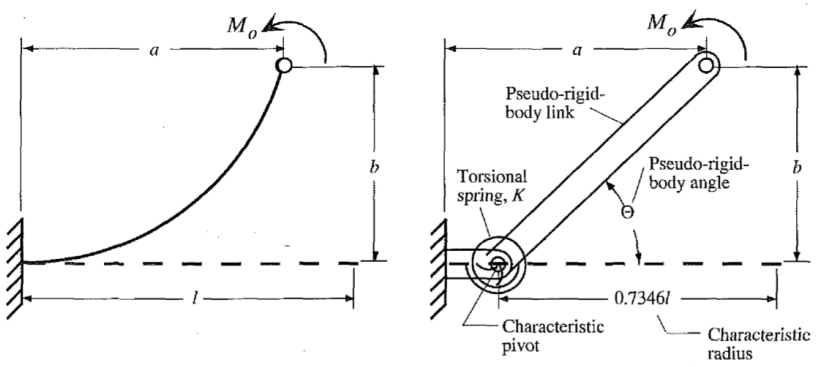

Figure A.1: The definition of the characteristic pivot for a cantilever beam with a moment at the free end [1]

To find the characteristic pivot, Howell matches the path of the endpoint per loading condition to a circle to minimise the error [1]. For a flexure with an applied moment, a circle with a radius of 0.7346 matches the path best. To then match the deflection rate, an angle coefficient is used. For this Howell comes to 1.5164, meaning that for a flexure angle of 1.5164° degrees, the PRBM linkage has an angle of 1°. Figure A.2 shows the green lines almost intersecting the endpoints of the flexure modelled by the arc method. Figure A.2 also shows the angle error of the PRBM, where the actual flexure attachment in black has a different angle than the characteristic pivot link in green.

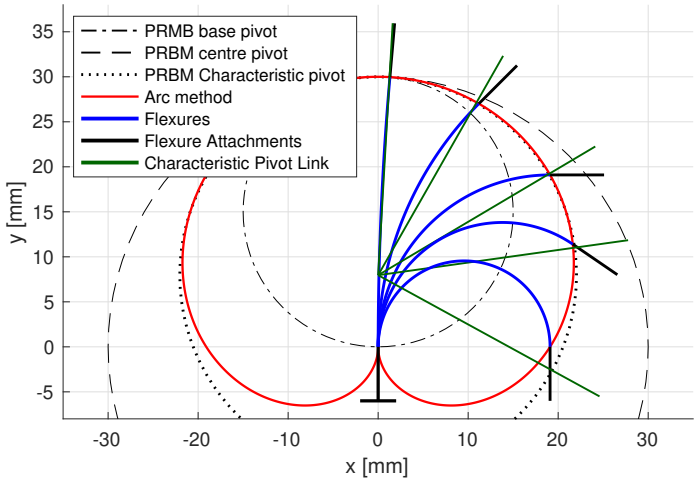

Figure A.2: The comparison between the arc method and three PRBM approximations. One with the pivot at the base of the flexure, one at the centre of the flexure and one at the characteristic pivot. Flexure shapes for four different output angles are also shown in blue, as well as the characteristic pivot with angle coefficient in green. The angles for these are: 5, 45, 90, 124.4, 180°. 124.4° is the maximum angle for which Howell specifies a position error of less than 0.5% of the tip deflection.

The increase in accuracy for the endpoint position can also be seen from figure A.3. For the first 124.4°, the characteristic pivot with angle coefficient matches the arc method. But again, when modelling accuracy of the system that attaches to the flexure is important, not only the endpoint position, but also the endpoint angle is important, for which the method now has an error.

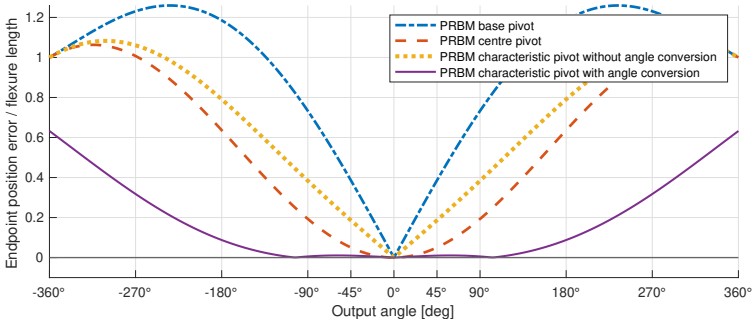

Figure A.3: The normalised error of endpoint calculated by the different PRBM methods against the actual flexure deformation calculated with the arc method plotted over the deformation angle. The PRBM methods without an angle coefficient all have an error of 1 at 360°, meaning a full flexure length of error. This is because the arc method correctly predicts that the flexure shape creates a loop at 360° deflection, having the endpoint and base of the flexure touch, while the circle paths of the PRBM methods rotate back to their starting position. Hence, a flexure length of error.

To correct this angle error, we propose an additional bend which can be added at the end of the link, bending back to the original output angle as is shown in figure A.4. However, this increases complexity substantially, as the distance between the PRBM pivots is now not constant anymore, but changes for different output angles, which can result in a necessity for an iterative solver in some systems.

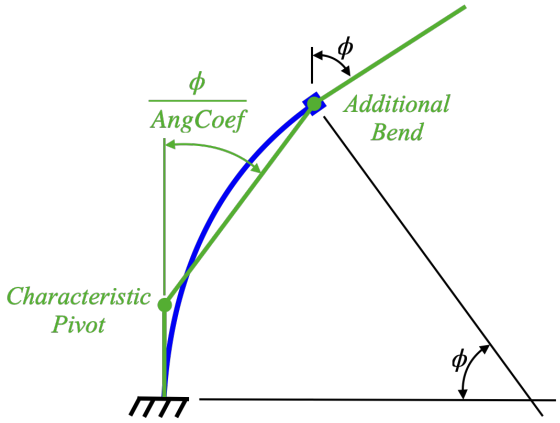

Figure A.4: The added bend to the end of the characteristic pivot approximation, bending back to the original output angle.

This method is also tested against the measurement data done for the TPU Flexure, and it does increase accuracy, as is shown in figure A.5. The PRBM with characteristic pivot, angle coefficient, and additional bend performs a lot better than the other PRBM methods, but still worse than the arc method.

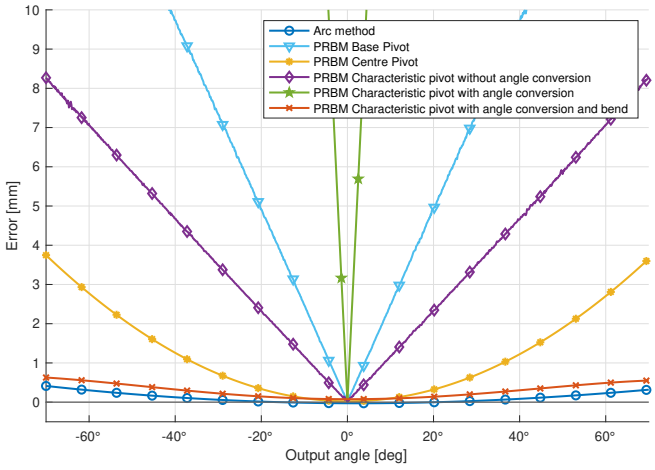

Figure A.5: The error of each of the PRBM methods. Each of the lines is a fitted average of data using a smooth spine fit. The lines for the PRBM base Pivot and PRBM Characteristic pivot with angle conversion continue linearly to ±70°. The same input angle is used for each of the models when calculating the error.

As the PRBM with characteristic pivot and angle coefficient is nothing more than the best fit of the actual flexure, another option arises. Not fitting only the flexure endpoint to best match, but both the flexure and attached system. This is also tried for the flexure with an attached rod. This is of course dependent on the ratio between flexure length and rod length. For a flexure of 30 mm with a rod attached of 400 mm, a characteristic pivot point at $(1-0.658)*FlexureLength = 10.26$ gives the best matching circle to the path of the endpoint. To then match the deflection rate, an angle coefficient of 1.013 is used. Figure A.6 shows this new optimised characteristic pivot location and angle coefficient. The results from this optimisation can be seen in figure A.7. Again, this technique is less accurate and more complex than the arc method.

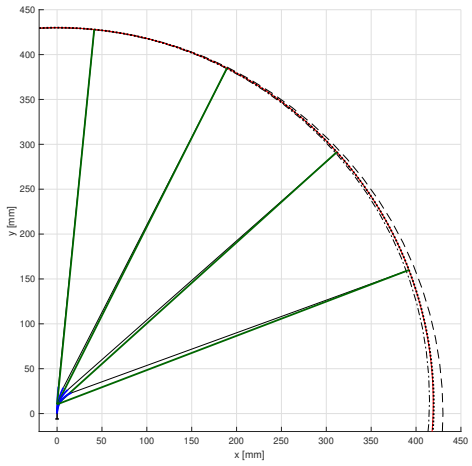

Figure A.6: The characteristic pivot of the flexure and attached rod for different deformation angles. The actual flexure and rod drawn in blue and black, with the PRBM approximations drawn in green.

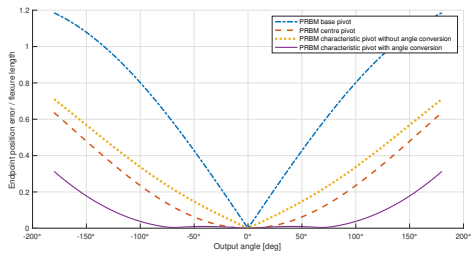

Figure A.7: The normalised error of endpoint of the flexure with attached rod calculated by the different PRBM methods against the actual flexure deformation calculated with the arc method, plotted over the deformation angle.

References

[1] Larry L. Howell. *Compliant mechanisms*. Wiley, 2001, p. 459. ISBN: 9780471384786.

Appendix B

Flexure Design and Implementation

This appendix documents the design of a polymer short wire flexure joint to replace a balljoint in a delta robot. The three production methods for the polymer flexures, 3D printing, casting, and using round stock, are looked into. they are then tested on a delta robot. hi

B.1 3D printing flexures

Next to inquiring literature on the subject, a more hands-on approach can also be very useful. With the 3D printer at Codian Robotics, a few simple test hinges are printed to check what sort of baseline we are working with. Using a simple flexure shape and some flexible printable material that is at hand, some tests are set up. For this first prototype, hinges are designed for a 3DOF Delta robot. The D4-1100 is chosen, as it is already set up in one of the testing machines at Codian Robotics.

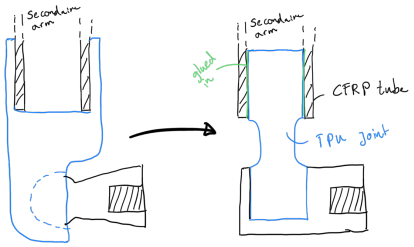

Figure B.1: A initial drawing of a flexure design

For this first test a notch flexure is used, as it is easy to 3D print, and one of the simplest, most used flexure shapes. The flexible material at hand is Ultimaker's Thermoplastic Polyurethane (TPU) 95A[1]. The diameter of the flexure is based on the inside diameter of the carbon fibre reinforced plastic (CFRP) tubes used in the linkages of the Delta robot, see figure B.1. A few

different notch geometries are printed, to test how far the joint can bent. One of these first test joints can be seen in figure B.2.

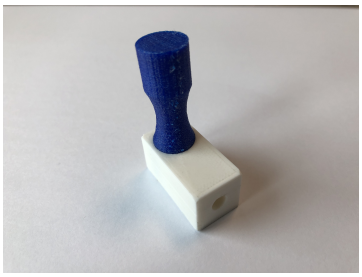

(a) The flexure and white connection adaptor, to connect the already existing screw point on the robot.

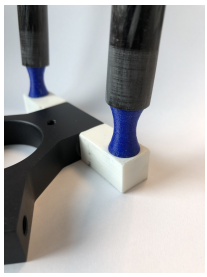

(b) The Flexure screwed onto an TCP, and inserted into a carbon rod.

Figure B.2: The first 3D printed notch flexures, made from TPU.

Based on the first tests, the following observations were made.

- *3D printing* - Although for more large scale production injection moulding could be considered, these first prototypes are made with a 3D printer. The following points are mainly about the properties that accompany 3D printing. But as the first few iterations will still be printed, it is still valuable to look into this.
- *Printing direction* - printed TPU is very flexible, but has a weakness due to the manufacturing method. The adhesion between the different layers of the 3D print is a weak spot. The first models were printed upright, so the layer lines were perpendicular to the flexure. This was done mostly for printability, as now no support structure is needed. This would be necessary when the model was printed laying down on its side. Also, this gives equal properties in both flexible directions, as when on its side there will be a difference between the two. However, now the highest tensile stresses are perpendicular on the layer lines, and cause the print to start tearing at too much bending.
- *Infill percentage* - The first flexure was printed with an infill percentage of 50%. This is quite standard for 3D prints, but caused some unexpected properties in the hinge. For large deflections, the walls buckled, as the structure was mostly hollow. This greatly lowered the stresses in the material and reduced the rotational stiffness. However, this hollow structure also caused a decrease in translation stiffness.
- *Material Selection* - The material characteristics, particularly ratio of Young's modulus vs yield strength, has a large effect oh the hinge geometry.
- *Attachment to TCP* - For easy prototyping, the hinges are made so that they can be screwed onto the existing mounting holes. The white blocks serve this purpose. Because in the TCP there is just a single tapped hole, the alignment of the blocks is not perfect, and a different system needs to be implemented.

Based on this, the model is altered, and some more tests are printed. For these test the same material is used, as this is easily available at Codian. The hinge geometry is altered, to be able to print the hinges laying down flat on their side. This makes the layer lines in line with the hinge and gives a stronger product. The first test can be seen in figure B.3a, where a bolt directly

fastens the flexure to the TCP. In this design, the bold could not be preloaded enough, due to the flexibility of the 3D print. A larger hole was printed, where a bushing could be glued in, see figure B.3c. This bushing can be preloaded on the robot.

(a) The altered design, which can be printed flat on the table

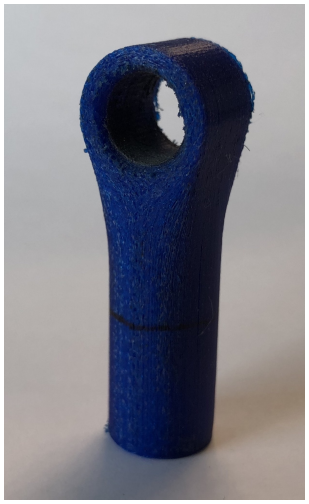

(b) The print with larger hole for a bushing

(c) The flexure glued into the carbon rod with a bushing

Figure B.3: 3D printed joints

The glue layer between the bushing and 3D print also came loose over time, so a different option was explored, multi-material prints. The places where the flexure has to be screwed to the system and glued into the rods are made from a stiffer polycarbonate (PC). This material was chosen as it should match and merge well with the TPU print.[2] PET-G was also used, but this merging with the TPU was worse than the PC.

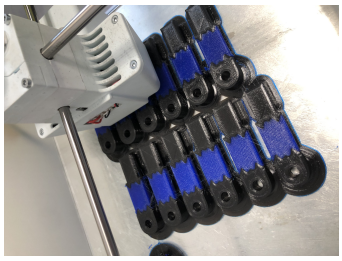

(a) A multimaterial 3D print of the flexures

(b) A print where the TPU Filament became blocked halfway. This shows the inside of the flexure

(c) A single TPU flexure, printed with white PC instead of the black PC in the two figures next to this one

Figure B.4: Multi Material 3D prints

These multi-material flexures held up a lot better over time. One problem that still persisted, however, was that some batches of flexures tore at the merge line between the two materials, as can be seen in figure B.5b. 3D printing is a manufacturing method for which it is difficult to

reproduce the same exact part with multiple prints. Variables like room temperature, moisture levels etc. can have a large effect on the quality of the print.

(a) The TPU is starting to tear (b) A torn of flexure

Figure B.5: Tearing of TPU and PC multimaterial 3D prints

B.2 Casting flexures

Casting flexures is also investigated. The same core as for the multi-material prints is now printed separately, which can be put into an also 3D printed mould to cast around. The core wire can be seen in figure B.6a, the mould in figure B.6b.

(a) The core of the flexure to pour around

(b) A 3D printed mould with cores inserted.

(c) Using a syringe to press the polyurethane into the mould.

Figure B.6: Casting flexures

Both silicone and polyurethane are tested for casting. Both of these did not yield any usable results. The silicon is difficult to merge to other parts, which makes it easy to remove from the mould, but difficult to attach to the delta robot. The two-part PU used was to brittle, not useful for this type of application. This could still be further explored, but in this research, as the 3D printed flexures yielded better results, it is not looked into.

(a) A silicon cast (b) A broken polyurethane cast

Figure B.7: Casting Results

B.3 Clamping flexures

To ease manufacturing, using solid polyurethane round stock was looked into. This is then clamped at either end using a bracket, as can be seen in figure B.8a. For this, Eladur was used.[3] In this setup, TPU 3D printed flexures were also tested, as only the merging to the PC was the issue for the 3D prints. These worked better than the PU round stock and were tested on the delta robot as can be seen in figure B.8b. These systems are designed to work with the already available bolt holes in the arms of the delta robot. If the system is designed for flexure hinges, the clamping system can be integrated in parts such as in figure B.8c. Here, a new type of TCP is shown with integrated flexure holders, which replaces the system as shown in figure B.5.

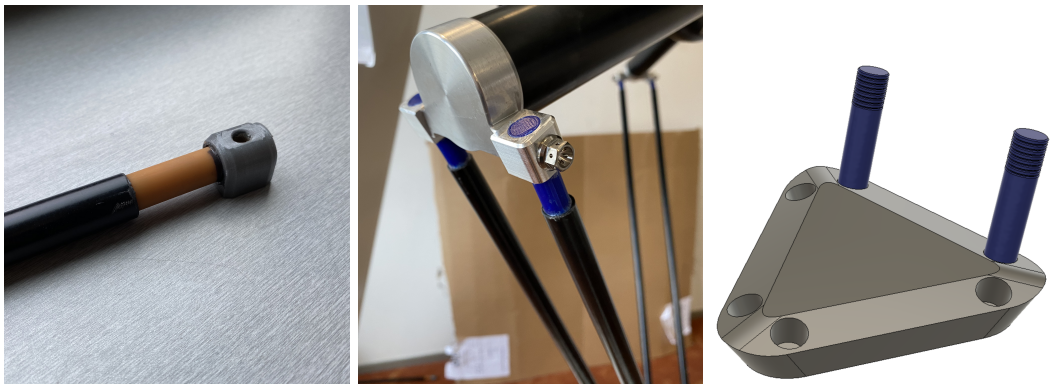

(a) A clamped PU rod (b) The clamped TPU flexures on the Delta robot (c) A new TCP design directly clamping the flexures.

Figure B.8: Clamping Flexures

B.4 Full Delta robot

The hinge design from figure B.3c can already be tested on a full-scale delta robot. 6 rods are made and are bolted on one of the test robots at Codian. When the motors are not locked, just by moving the TCP by hand, the whole workspace can be tested. There is some stiffness in the system due to the deflection in the hinges, but no clear problems.

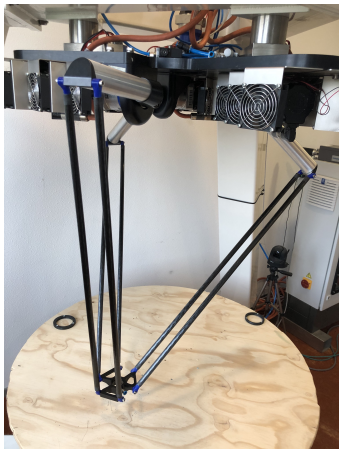

(a) The Delta robot with flexible couplings

(b) A close up of the couplings on the primary arms

(c) A close up of the couplings on the TCP

Figure B.9: Flexible delta robot

At the end of the tests, the flexures were already somewhat warm. The internal friction of the material slowly heats the flexures as the robot moves. Still, some modelling and testing need to be done to check what the steady-state temperature is for these flexures. However, the bushings came loose over time.

The multi-material flexure was also tested on the delta robot. These worked quite well, reaching pick and place speeds of over 400 picks per minute over a path of 600mm wide and 200mm high. This is twice the speed of the fastest robot that Codian has made so far.

Finally, the clamped solution was tested. This test is still going on today, reaching a bit slower pick and place speeds then the multi-material flexures as the mounting is heavier, but with better durability. As of now, this test has run at 200 picks per minute for 48 hours, resulting in over half a million of pick and place cycles.

References

[1] *Ultimaker TPU 95A material: 3D print durable and flexible parts.*
[2] *How to print with Ultimaker TPU 95A – Ultimaker Support.*
[3] *ELADUR Federelemente — Alfred Konrad Veith GmbH & Co KG.*

Appendix C

Feed Forward Model with Arc Method for Delta Robot

First, the inverse kinematics for a delta robot with rigid joints, like ball joints, is be explained. This model is then altered to use the arc method to better feed-forward predict a delta robot with flexures.

C.1 Inverse kinematics for Delta robot with rigid joints

The delta robot can be directly solved, both with forward and inverse kinematics. In real-world use cases, the inverse kinematics are the most useful. These calculate the position of the three input arms based on a location of the TCP. This seems like a complex, 3-dimensional problem where 3 arms need to be solved simultaneously. However, it is not. More specifically, it does not have to be solved simultaneously, and in essence, it is not a 3D problem. The parallel nature of the delta robot makes sure that the end effector cannot rotate. This means that each of the three arms can be solved separately, as it is a fully determined kinematic chain from the attachment on the end effector to the base. When solving this single arm, a smart choice of coordinate system can reduce the solving to only a 2D problem. With the Z-axis pointing straight up, and the X-axis to be in line with a primary arm, such that the primary arm rotates around a line parallel to the Y-axis. Because the primary arm can only rotate around this axis, the problem can be flattened to only the XZ-plane. Because of the axis system, the Y coordinate of the TCP can be set to zero for the desired effect, as can be seen in figure C.1a. From here the cosine rule is used to find the angle of the upper arm. The cosine rule calculates the angle of one corner of a triangle when all sides are known. This is the case here, as we know the distance between the base and TCP, the length of the primary arm and the length of the projected secondary arm. This projection on the XZ plane is illustrated in figure C.1b. With this model, a single arm can be solved for any TCP location. Due to the symmetry in the delta robot, only the coordinate system has to be rotated 120° to solve the other arms.

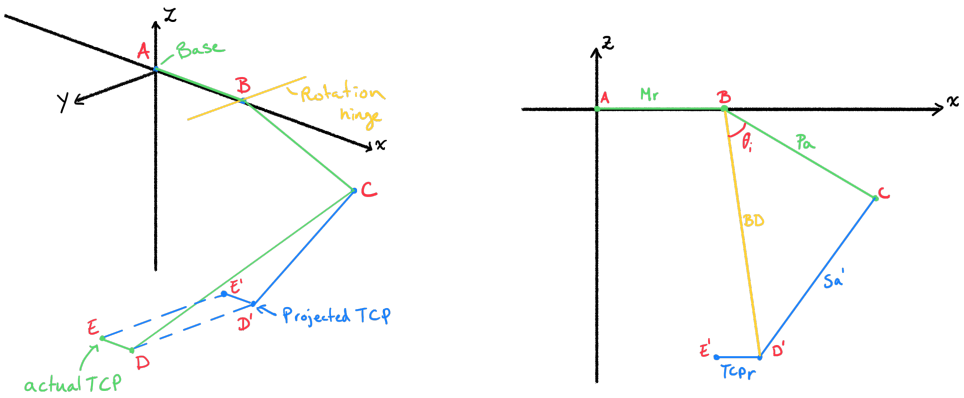

(a) The inverse kinematic solver principle

(b) The 2D solving method using the cosine rule

Figure C.1: Inverse kinematic model

To find the joint angles for the ball joints, a simple parabolic path with a distance of 1200 mm and a height difference of 300 mm is used, see figure C.2.

During this action, the joint angles both inplane, θ_1 and the angle out of plane θ_2 are measured. This is done for each of the links.

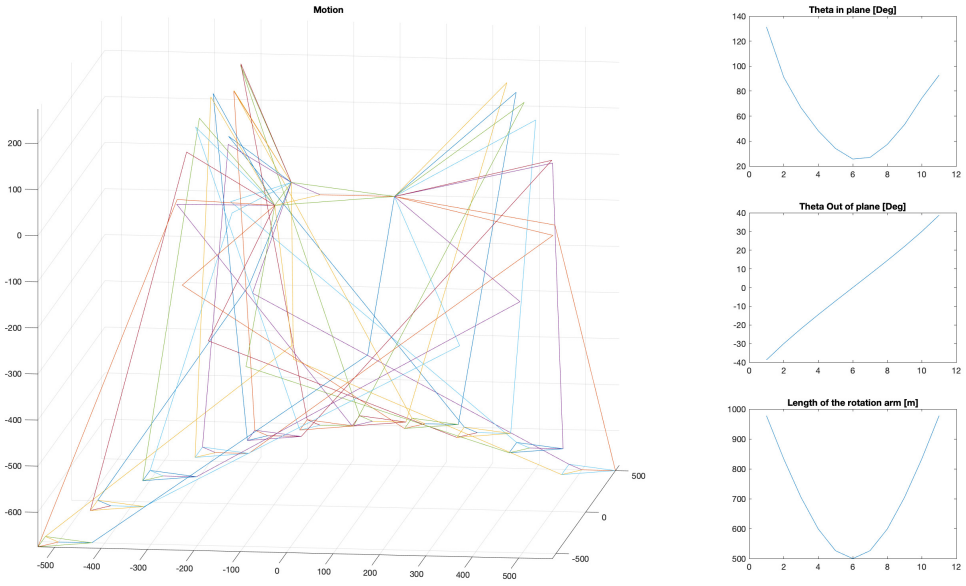

Figure C.2: A parabolic path of the TCP with the different joint angles and rotation arm lengths.

C.2 Inverse kinematics with arc method

The modelling done in the previous section revolves around perfect ball joints, that allow only rotation and no translation. However, if these joints would be replaced by flexures, the rotations also come with some amount of translation. These translations have to be modelled to accurately predict the position and motion of the robot. As the Delta robot is feed-forward controlled, the correct prediction of the position of the robot is necessary. The TCP position of the robot is controlled by the length of the secondary arms, meaning that the length changes that the flexures introduce have an effect on the position. For this model, we start with the simple flexures or short wire flexures used in the prototypes of the flexible Delta robot. As they are the same thickness over their entire length, a moment on the flexure causes a circular bending radius. External forces on the flexures cause a deviation from this circular deformation, as for imperfections in the flexure or accelerations of the robot. For the first model, the hinges are approximated by a circular arc of a set length. A simple back of the envelope calculation shows that this change in for a 20mm long flexure, and a 20 degree bend the length of the secondary arm changes significantly. This is enough to require a different set-point for primary arms higher than the precision of the motors.

If the robot is used only between two points, these two points can be calibrated and still feed-forward controlled. However, when the robot needs to move accurately in a 3D space, calibrating every point is not efficient. Then, using the arc method to predict the hinge deformations and change the kinematic model is more efficient. To implement the modelling approach, each joint is replaced by a circular arc, as can be seen in figure C.3a To model the system, the virtual centres (VC) are determined for all flexures, as can be seen in figure C.3b. For the feed-forward model, the position of the end effector is known with respect to the base, and the angles of the primary arms are the output of the inverse kinematic model. Even though the system is build up from simple elements, a solution as simple as the one for the delta robot without flexures is not reached. An iterative solver is used to solve the system of equations for the angle of the primary arm.

C.2.1 Iterative solver

For the delta robot with flexures, the assumption that the end effector of the delta robot, the TCP, stays parallel to the base is still valid. Of each of the lower arms, the two flexures deform in the same fashion in every direction, thus make sure that the parallelogram of the lower arm is still parallel. This means that each arm can still be solved separately, just as for the delta robot with ball joints. However, as stated before, an iterative solver is used to solve each of the arms of the delta robot. This solver works as described in the following steps:

1. An arm of the delta is solved as if none of the flexures are deformed, and the VC lies halfway each flexure. This means that the arm with flexures can be solved just like the regular robot, but now with ball joints at the VC positions
2. The angles of each of the joints are calculated based on the solve from step 1, and the positions of each of the VCs are altered. The arm is then solved again based on these new VC positions.
3. Step 2 is repeated based, each time giving a better prediction of the angle of each of the flexure joints.
4. The error between each step is calculated as the change in primary arm rotation, as this is the input of the system. The motor is attached to the primary arm. When this error is

smaller than the precision of the motor and gearbox, the loop is stopped. This takes 2 or 3 iterations, based on the endpoint position.

5. This is then done for the two other arms in a similar fashion.

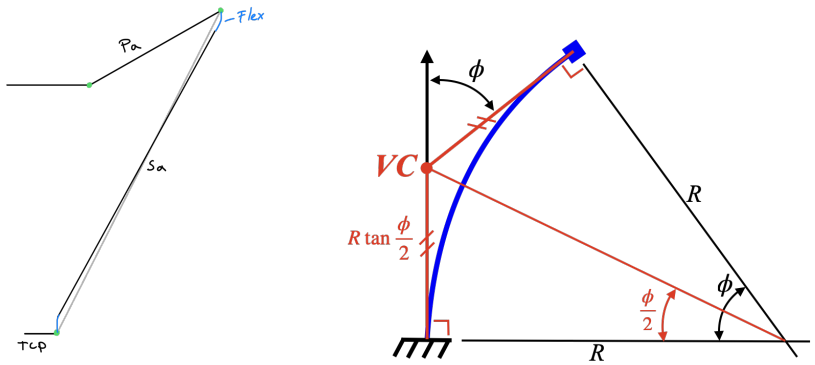

(a) Sketch of delta robot

(b) Virtual centre for ease of modelling using arc method

Figure C.3: Sketches of kinematics

The final Matlab model can now quickly feed-forward predict the position of the TCP or end effector of the delta robot.

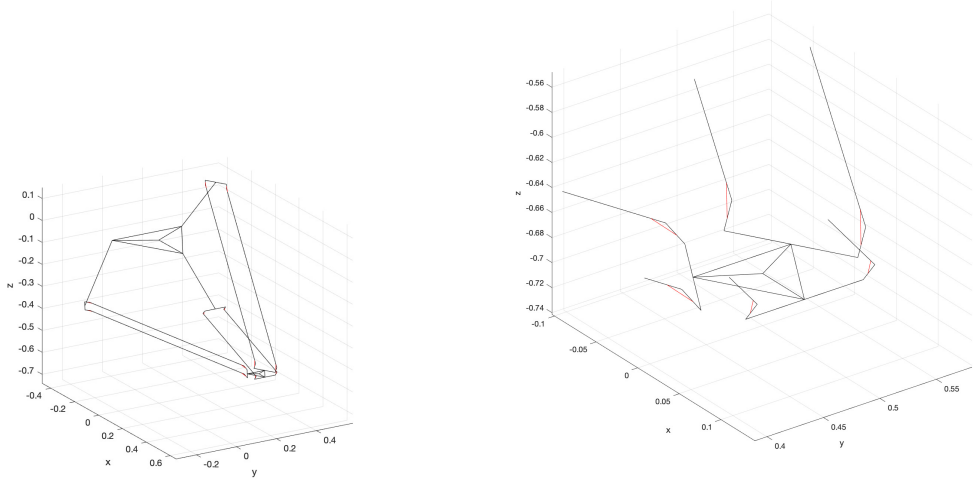

(a) An overview of the kinematic model

(b) A zoomed in view of the TCP of the robot. The flexures are shown as red lines, as drawing arcs in Matlab is not efficient

Figure C.4: Matlab model of Delta robot with flexures based on arc method

C.3 Testing

This model is measured against a real-world system. This is done by positioning the end effector of the delta robot with flexures with to a know location in 3D space, and measuring the angles of each of motor positions. This location is calibrated with the same delta robot, but with rigid linkages. This way of measuring with the rigid delta robot has an error of maximum 0.1 mm. The inverse model is then used to also calculate the angles of the motors from this know position of the end effector. The maximum difference between the calculated and real-world values is 0.01° at the motors. This error would result in a position difference on the end effector of 0.06 mm, which is within the measurement accuracy of the test.

Figure C.5: The calibration of a point in 3D space to test the feed forward model of the delta robot with flexures.

C.4 Other solving methods

Other methods were tried to directly solve the delta robot with arc methods, but none succeeded. No direct solution was even found for the 2D problem is sketched in figure C.6. Different iterative solutions were found, however, but the method using the VCs showed the most potential of working in 3D. Here a shortlist of other approaches that worked iteratively in 2D

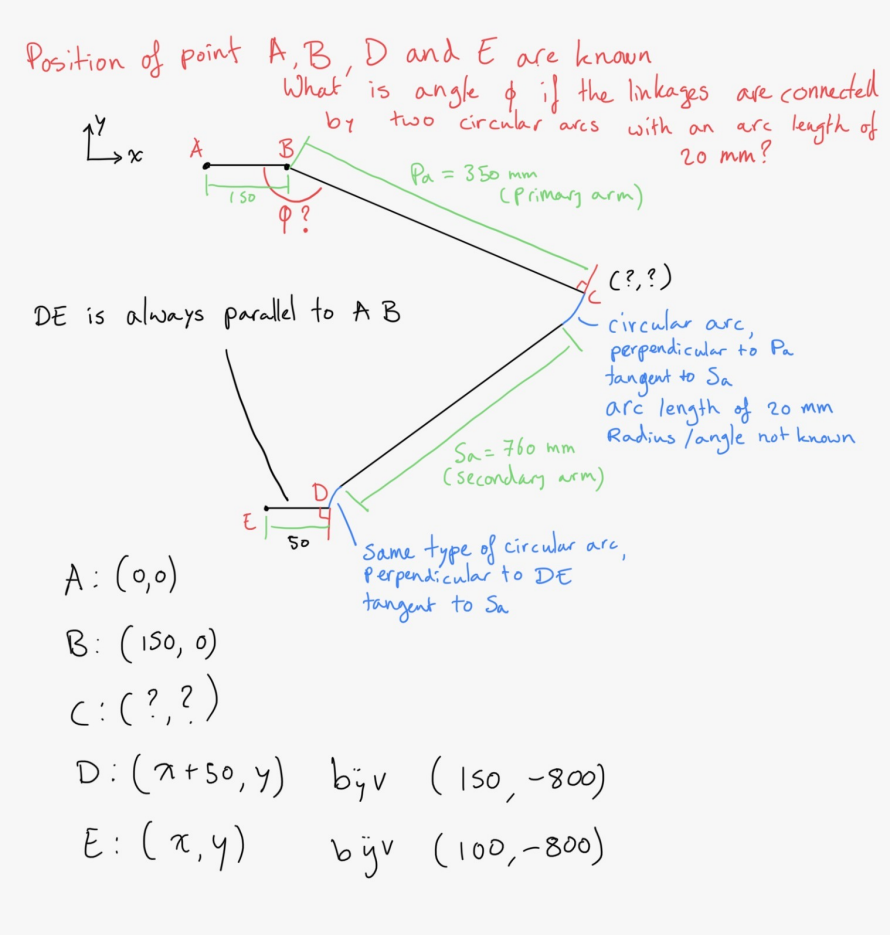

Figure C.6: The 2D problem statement for the inverse kinematic model of a delta robot. Here the out of plane component of the arm is not yet taken into account

C.4.1 System of equations

Building a system of equations: an equation for both the X and Y coordinate of the TCP can be made, based on the angles of both of the flexure joints. These two equations can then both be iteratively solved by setting them equal to the actual X and Y coordinate of the TCP that is required. The equations that are reached are then as follows. These equations cannot be directly solved, thus a numeric solver is used. In these equations, the parameters from figure C.6 are used, with the following added: l is the length of the flexure, γ Angle between the Sa and DE, and C_{Flex} is the point under C after the flexure.

$$C = B - (Pa + l/(\phi - \gamma - \frac{\pi}{2}) * (\sin\pi + \gamma - \phi - 1)) * [\cos\phi; sin\phi] \quad \text{(C.1)}$$

$$C_{Flex} = C - (Sa + l/((\phi - \gamma - \frac{\pi}{2}) * \tan\pi + \gamma - \phi) + l/((\frac{\pi}{2} - \gamma) * \tan\gamma)) * [\cos\gamma; \sin\gamma] \quad \text{(C.2)}$$

$$D = C_{Flex} + [l/(\frac{\pi}{2} - \gamma) * (1/\sin gamma - 1), 0] \quad \text{(C.3)}$$

C.4.2 Other geometric methods

Other ways of solving the delta robot based on the geometry of the arc were tried, such as looking at the intersection of the different parts of the delta robot arm. This is done by extending the secondary arm Sa until it intersects with the primary arm for the top flexure, and with the line through the TCP for the bottom flexure, as can be seen in figure C.7a. The equations for such an intersection can be seen in figure C.7b. This gives a system that is closer to the rigid delta robot again, and can thus be solved like one. This solution is then iterated to find the solution.

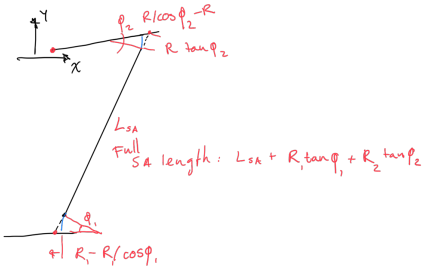

(a) The intersection of the different arms.

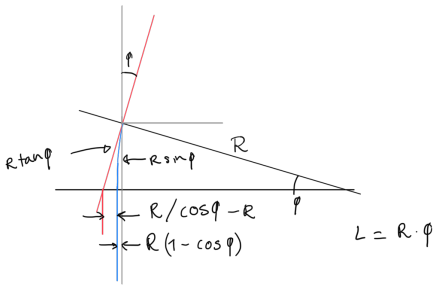

(b) An intersection method with the hinge perpendicular to the arm.

Figure C.7: Intersection method

This method can also be extended to work with flexures that are not bolted on perpendicular to the arms, but at an angle. The equations for this can be seen in figure C.8. This method also worked in the 2D system. Implementing it in 3D space proved more difficult, as these intersections now would not lie in the same plane anymore. Overall, the method using VC was simpler and therefore chosen as the modelling mechanic.

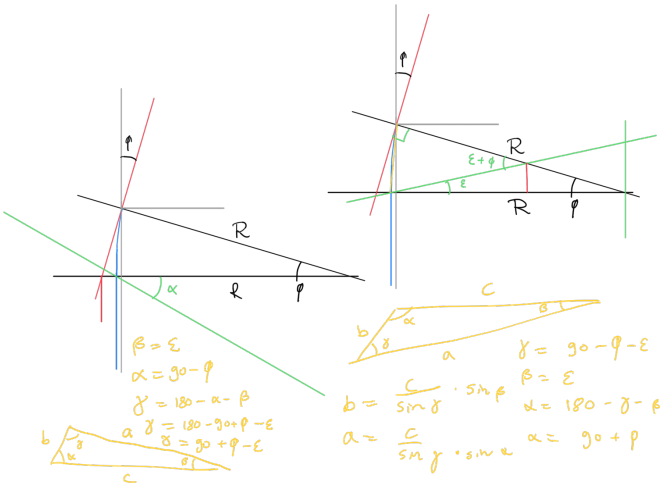

Figure C.8: An intersection method with the hinge perpendicular to the arm.

Appendix D

Compliant Rotation Shaft for the Delta Robot

Next to replacing the ball joints with flexures, the rotation shaft is also looked at. The rotation shaft of a delta robot is used to add a 4th DOF to the end effector. A normal delta robot can only move the end effector in X, Y and Z, but by adding a rotation shaft, the rotation around Z can also be changed. The rotation arm is build-up of two U joints and a linear bearing, as can be seen in figure D.1b.

(a) A D4 Delta robot with 4 DOF, using a rotation arm.

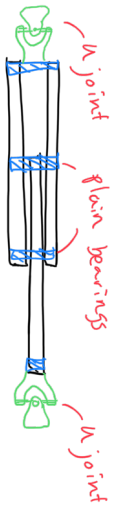

(b) The Rotation arm of a D4 robot, with a U joint and linear bearing

Figure D.1: Delta robot with rotation arm

Some initial research is done to replace both the U joints and linear bearing with compliant mechanisms. Both of these joints suffer from the same problems as the ball joints, difficulty to clean. A first design is made based on the joints from Trease (2005).[1]

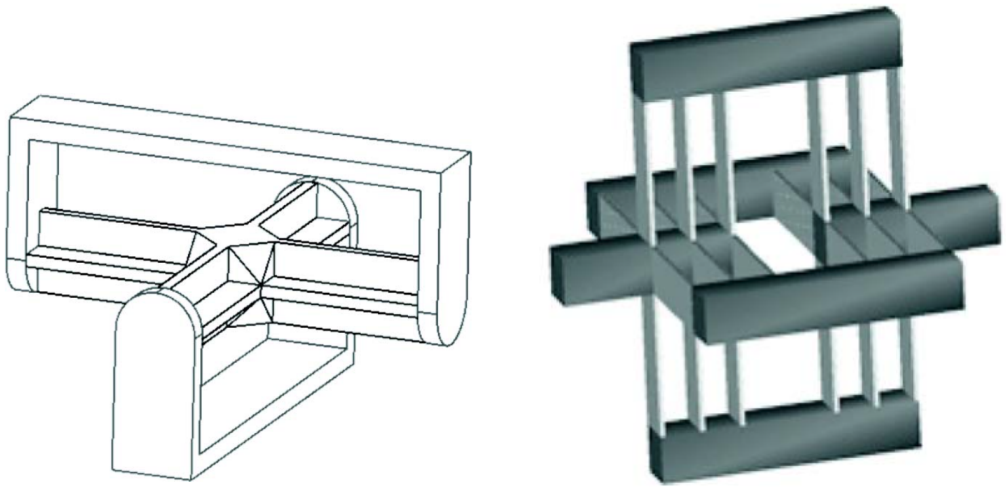

(a) The U joint with 2DOF, to replace the U joint in the rotation arm

(b) A translational joint, to replace the linear bearing

Figure D.2: Possible joints to make the rotation arm compliant [1]

However, based on these joints, a new idea was formed. To combine both of these joints into a single joint. This removes constraints from both of the joints, opening the possibility to different flexure types. The joint has to only constrain rotation around the Z-axis, while being free in rotation around X and Y, as well as translation along Z. Translation in X and Y should be constrained to some amount, as otherwise, the whole rotation arm could move independently from the robot.

First prototypes of this joint are made from paper, as can be seen in figure D.3 Two of these joints would be required, one at the bottom and one at the top of the rotation arm, replacing both the U joint and the linear joint.

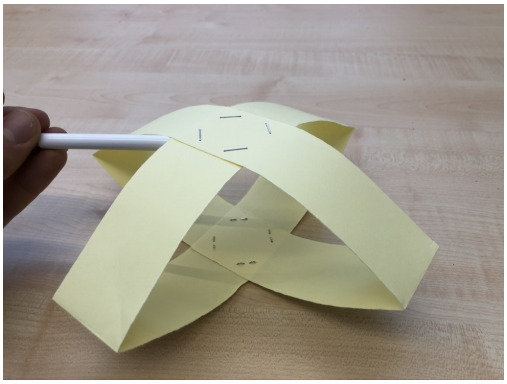

(a) Here the top and bottom of the crossing leaf flexures would be connected to the the input and output axles, limiting rotation around Z and movement in X and Y

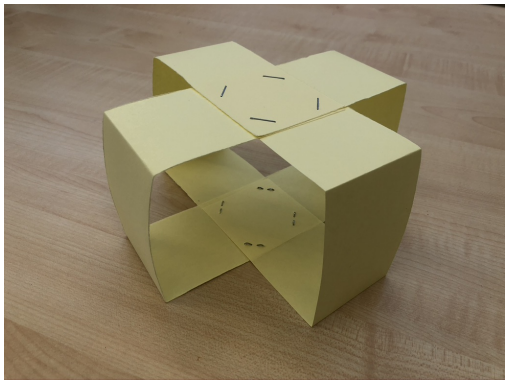

(b) Working in the same way as D.3a, but as the two crosses of leaf flexures are now spaced, they can bend in either direction, increasing movement range.

Figure D.3: Paper prototypes of a rotational and translational joint

Prototypes using steel leaf flexures and 3D printed parts were made and tested. The Flexure cross with spacers has the largest range of motion so that one is studied in more detail.

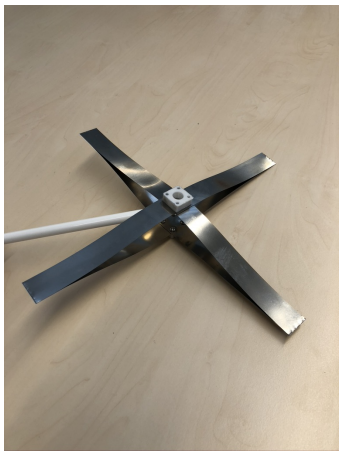

(a) A flat crossed leaf flexure. A pen is used to keep the two sides slightly spaced apart

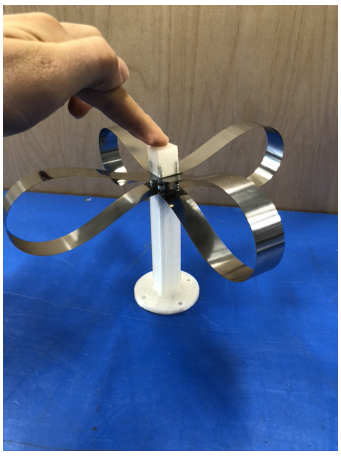

(b) A bend crossed leaf flexure

(c) A spaced crossed leaf flexure

Figure D.4: Flexible delta robot

A problem with the version where the two crosses of leaf flexures are spaced is that the intermediate bodies could be rotated when stressed, as can be seen in figure D.5a. Additional flexures are added between these intermediate bodies to prevent this from happening.

(a) The rotated intermediate bodies

(b) Stiffener flexures added

(c) Stiffener flexures with a sharp bend

Figure D.5: Flexible delta robot

This flexure has both a large range of motion in the Z direction and in rotations around X and Y, but is stiff in the rotation around Z and in the motion in X and Y. This means it could be applied to a delta robot. The render below shows how this could be implemented, although the added stiffener flexures are still missing there.

(a) full view

(b) bottom view

Figure D.6: A render of the design of a delta robot with compliant rotation arm

References

[1] Brian P. Trease, Yong-Mo Moon, and Sridhar Kota. "Design of Large-Displacement Compliant Joints". In: *Journal of Mechanical Design* 127.4 (July 2005), p. 788. ISSN: 10500472.

Appendix E

Test Setups

E.1 Support stiffness test

An attempt was made to validate the support stiffness model with a tensile test bench, as can be seen below. The flexure is first bent to a certain deflection angle, after which it is loaded to determine it's support stiffness in that direction. This setup with the long rod attached to the flexure means that the endpoint of the flexure can move in X and Y direction while being loaded in the Z direction. This is comparable to how flexures are loaded in the delta robot, where only the angle of the flexure is an input.

(a) The scale used to input an deflection angle on the flexure

(b) a closeup of the upper clamp used

(c) The deformed flexure ready to be tested.

Figure E.1: Test setup to test the support stiffness of the TPU Flexure

However, due to a problem with the sensor of the tensile test machine, the results of this test are not very accurate. The problem was probably a low stiffness of the sensor of the test machine

itself, but this still has to be checked. Overall trends can be seen, such as in figure E.2, where the support stiffness decreases for larger deformation angles.

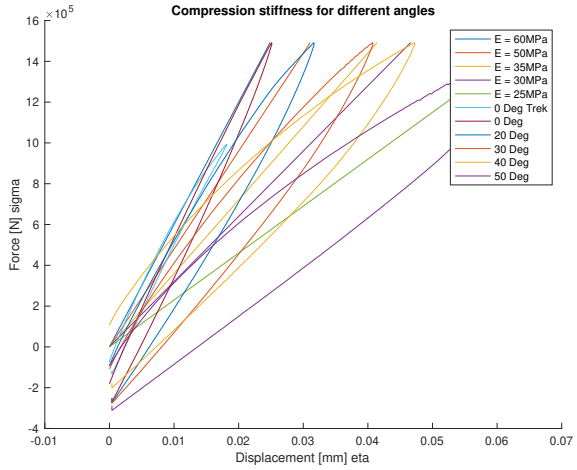

Figure E.2: Compression stiffness, the deflection normalised to the length of the flexure (clean up this graph)

Multiple tests were also done for the steel wires, but here the error of the tensile testing machine made that these tests were not usable. Another problem with this setup is that the top of the flexure is clamped in to lock the angle of the flexure, but this is also locking the position of the top of the flexure. This adds stiffness to the flexure, which is not modelled.

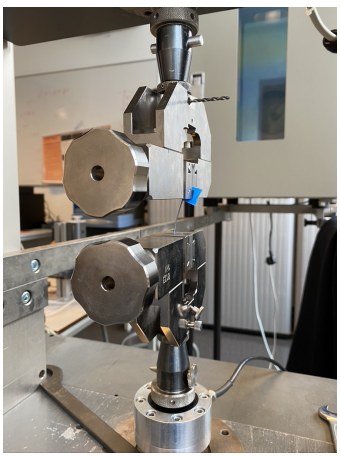

(a) An overview of the setup

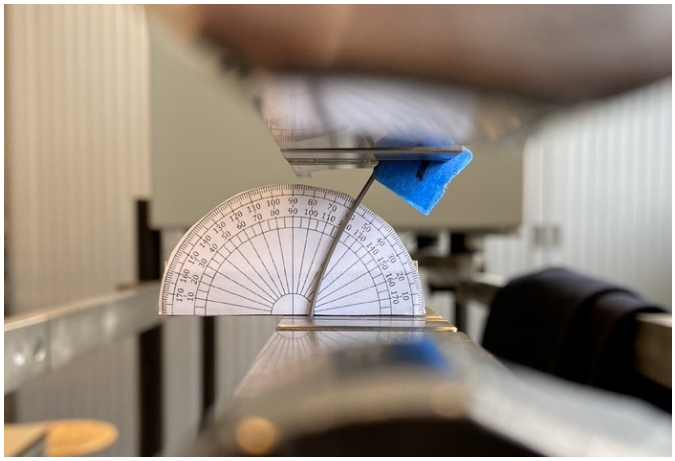

(b) A bend steel flexure

Figure E.3: Steel wire tests

E.2 Arc method test

To test the arc method, the delta robot was used to measure the deflection path of a flexure. This path could then be compared to the calculated path by the arc method. A flexure was fixed to a measured location on the bed of the delta robot. The end of the extension rod was then attached to the rotation arm of the delta robot, so it was free to rotate while moving around. The flexure was then deflected to either side by moving the TCP of the delta robot by hand. Both the rotation and position of the endpoint was measured. However, the amount of hysteresis in the rotation sensor setup was to large to yield any useful results. The position measurements did give useful results, as can be seen in figure E.5.

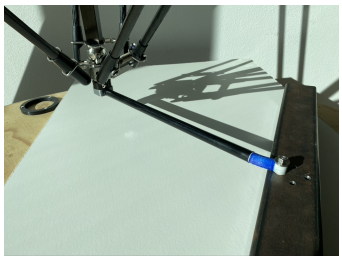

(a) An overview of the setup

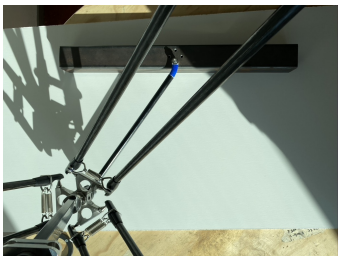

(b) A top view of the setup

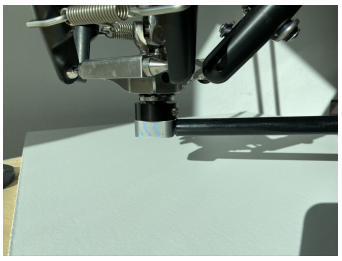

(c) A close up of the attachment to the delta robot.

Figure E.4: The use of a delta robot to measure the path of a TPU Flexure

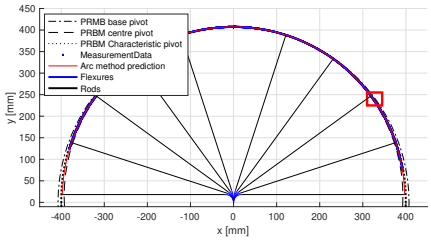

(a) The position of the endpoint of a rod attached to a 3D printed TPU flexure, with a few flexure and rod positions drawn in.

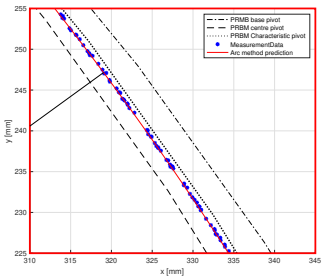

(b) A zoomed in section from the red rectangle from figure E.5a.

Figure E.5: The measurement results